Encounter Models for the Littoral Regions of the National Airspace System

M.W. Edwards

15 September 2010

Lincoln Laboratory
MASSACHUSETTS INSTITUTE OF TECHNOLOGY
LEXINGTON, MASSACHUSETTS

20100927138

The 66ABW Public Affairs Office has reviewed this report, and it is releasable to the National Technical Information Service, where it will be available to the general public, including foreign nationals.

This technical report has been reviewed and is approved for publication.

FOR THE COMMANDER

Gary Tutungian
Administrative Contracting Officer
Acquisition Enterprise Division

Massachusetts Institute of Technology
Lincoln Laboratory

Encounter Models for the Littoral Regions of the National Airspace System

M.W. Edwards
Group 42

15 September 2010

Lexington   Massachusetts

This page intentionally left blank.

EXECUTIVE SUMMARY

Airspace encounter models capture the complex geometry and behavior of aircraft after standard separation assurance has failed. Encounter models are essential to unmanned aerial system (UAS) sense and avoid (SAA) system safety evaluation. A SAA system with a demonstrated level of safety using extensive simulation and flight test evaluations will be required for unmanned aircraft to gain greater access to the National Airspace System (NAS). The Department of Homeland Security (DHS) strives to operate unmanned aircraft in the littoral regions of the continental United States (CONUS), but recent encounter models do not explicitly distinguish littoral traffic from other traffic. The framework and data used to build previous airspace encounter models for the NAS were used to develop encounter models for the littoral regions of the NAS. Since this existing framework was leveraged, the littoral models were directly compared to existing models to ensure that they had both sufficient data and distinctive characteristics.

The primary product of this analysis was the development of a littoral correlated and uncorrelated model for use in SAA system evaluation. In addition, a methodology was developed to determine whether the models were both distinctive from their CONUS counterparts and sufficient in terms of the quantity of data used to build the models. Application of this methodology demonstrated that both the littoral correlated and uncorrelated model characteristics were different than the previous CONUS models and that sufficient data were used to build the models. Specifically, it was found that aircraft flying under visual flight rules in the littoral environment have higher airspeeds and were observed at higher altitudes. Aircraft in littoral correlated encounters have higher airspeeds but encounters tend to occur at lower altitudes than those in the NAS. Lastly, this analysis determined that although the encounter initial conditions tend to be different in a littoral environment, the aircraft dynamic behavior, or how the various aircraft states transition during the encounter, remains the same.

Several future needs were identified regarding the airspace encounter model effort to support UAS SAA development and certification for current and future DHS missions:

1. Develop and demonstrate a methodology for characterizing the littoral non-cooperative density using existing radars. This is a required parameter for estimating the expected encounter rate and subsequently estimating the near mid-air collision (NMAC) rate—required for a target level of safety safety analysis.

2. Update the littoral model characteristics as the airspace changes. The Federal Aviation Administration's Next Generation Air Transportation System (NextGen) and the integration of unmanned aerial systems into the NAS will likely change both the traffic density and the attributes of the encounter models.

This will require monitoring the airspace continuously, and releasing updates as the model parameters change.

3. DHS maritime UASs will likely operate beyond the littoral environment. Thus, encounter and density models specific to the oceanic environment should be formed. This effort will require additional sensors that have coverage of the desired operating environment and that extend beyond those used for the CONUS and littoral models.

ACKNOWLEDGMENTS

This page intentionally left blank.

TABLE OF CONTENTS

LIST OF ILLUSTRATIONS

This page intentionally left blank.

LIST OF TABLES

This page intentionally left blank.

1. INTRODUCTION

Airborne safety critical systems must undergo extensive validation under realistic conditions prior to certification in the National Airspace System (NAS). Collision avoidance systems for manned aircraft, and the associated sense and avoid (SAA) systems for unmanned aerial systems (UASs), provide a safety critical function—ensuring separation when other safety layers (e.g., the underlying airspace structure, airspace procedures, and air traffic control), have failed to maintain separation. These complex systems are assessed in realistic large scale Monte Carlo simulations and flight tests to prove that they meet the desired levels of safety. Fundamental to these simulations is the use of realistic encounter situations between aircraft which are defined by the relative geometry and behavior of the aircraft during the encounter. The geometry and dynamic behavior of aircraft during encounters are captured in encounter models that provide a statistically sufficient set of features which are estimated from a large collection of observed encounter events. The initial and continuing evaluation of the Traffic Alert and Collision Avoidance System (TCAS) for manned aircraft illustrates the necessity of encounter models to estimate system effectiveness in a wide variety of encounter geometries [1–4]. This system evaluation methodology using encounter models for system assessment is required by ICAO when estimating TCAS safety risk [5].

There are fundamentally two types of encounters: correlated and uncorrelated. In the first type, at least one aircraft in the encounter is receiving air traffic control (ATC) services, and both aircraft are transponder equipped. In the second type, ATC services would no longer be provided because either one aircraft is not transponder equipped or both aircraft are flying under visual flight rules (VFR). The first type is termed "correlated" because there is active coordination provided by ATC prior to the loss of separation. It is therefore critical that the model capture this coordination between aircraft prior to the loss of separation. In the second type of encounter, a lack of ATC services results in uncoordinated loss of separation, hence these encounters are termed "uncorrelated"—i.e., aircraft blunder into one another. This uncorrelated feature is exploited by modeling each aircraft individually and then simulating the uncoordinated loss of separation.

Lincoln Laboratory recently built a set of correlated and uncorrelated encounter models for conventional and unconventional aircraft [6–8]. Unconventional aircraft are defined here as aircraft unlikely to carry transponder equipment—e.g., gliders, ultralights, balloons [9]. These models were intentionally created for the continental United States (CONUS) from a nearly national coverage of radar sensors. Data from these 134 radars, composed of long-range ARSR-4 and short-range ASR-8, ASR-9, and ASR-11 radars, were obtained through the U.S. Air Force's 84th Radar Evaluation Squadron (RADES) at Hill Air Force Base in Utah. The theoretical horizontal sensor coverage is shown in Figure 1—this illustration assumes the sensor specification for detection range without terrain masking. The data in the original uncorrelated model were collected during the time periods spanning 1–7 December 2007 and 1–7 June 2008 while the data for the correlated model spanned December 1, 2007 through August 31, 2008. Although the data to support the uncorrelated model were captured over the identical time period as for the correlated model, the data quantity during this two week time period was determined to be sufficient. These original encounter models are termed the "CONUS" models.

A SAA system which meets a specified level of safety will be required for consistent and widespread UAS operations in the NAS [10]. Encounter models are used to characterize the performance of
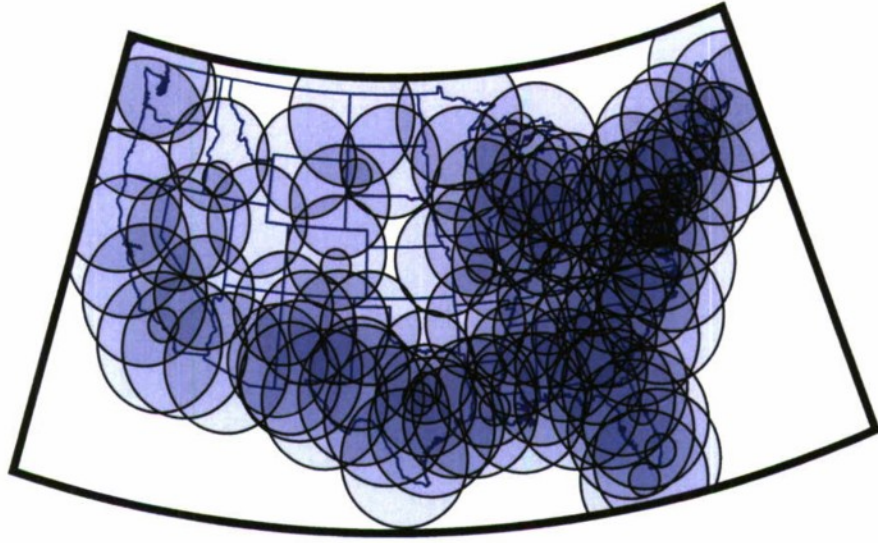
Figure 1. Radar coverage map.

the SAA system in the expected UAS operational environment. The Department of Homeland Security (DHS) has identified the need for UAS operations in the littoral regions of the NAS to support the missions of the U.S. Coast Guard and Customs and Boarder Protection [11]. Because of this identified UAS need, and the requirement to characterize the airspace for proving SAA system effectiveness, an encounter model specific to the littoral regions is desired.

Although the CONUS encounter models implicitly incorporate the littoral regions of the NAS, they do not separate the littoral region explicitly and do not therefore, capture the differences that may be expected in the encounter characteristics. For example, it is expected that a littoral model would capture terminal traffic when a major airport, or its arrival and departure routes, is located within or near the littoral region (e.g., Boston, Los Angeles, Miami). Because of the oceanic proximity of these terminal areas, there may be different encounter characteristics than terminal areas residing elsewhere. In general, littoral air traffic is expected to be less dense than other CONUS regions and have fewer instances of aircraft training and aerobatics.

The primary objective of this report is to present a methodology for forming correlated and uncorrelated encounter models specific to the littoral regions of the NAS. These models are created using a similar methodology and the data previously obtained and processed into the CONUS models. These models will be made publicly available and in a format compatible with the CONUS models. Although discrete- and 1200-code (VFR) traffic is observed in the littoral regions, very little unconventional aircraft traffic was observed. Hence, the focus of this document is the creation of a correlated and uncorrelated conventional model. The uncorrelated model capturing conventional (VFR) traffic will be referred to as the uncorrelated model for brevity. Because the data span the same duration and the geographic domain remains the same for the littoral and CONUS models, a separate description of encounter and traffic density is unneeded.

Before describing the approach for building the models, a definition of the littoral regions is required. The Department of Defense (DoD) defines the littoral environment as follows [12].

2

The littoral comprises two segments of operational environment:

1. Seaward: the area from the open ocean to the shore, which must be controlled to support operations ashore.
2. Landward: the area inland from the shore that can be supported and defended directly from the sea.

Because this model is primarily intended for use when developing and certifying UAS deployed to support the DHS maritime mission, the littoral environment is broadly defined as the area from the U.S. coastline oceanward to international waters (approximately 200 NM from the coastline).

1.1 DOCUMENT OVERVIEW

This report describes the process for modifying the existing CONUS encounter models to reflect the littoral airspace. This document does not describe the complete process for processing the radar data into the encounter models, but the process is identical to that described in the reports detailing the CONUS models. This document also assumes that the reader is familiar with the process for creating and subsequently using the encounter models. For a brief, high level discussion of the models, refer to [13–15]. The main text of this document does not discuss Bayesian networks, although Appendix E is included to describe the associated nomenclature.

Section 2 first presents the approach for filtering the radar data to extract littoral data. This section then presents the methodology for comparing the CONUS model to the littoral model and to confirm the distinct use of the littoral models. It concludes with a discussion on determining the sufficiency of the data collected by presenting metrics for model convergence.

Sections 3 and 4 describe the models that were generated and then carries out the model comparison and model convergence methodology of Section 2 for the uncorrelated and correlated models, respectively. The candidate model structures, graphically representing the conditional dependences between the model variables, are presented in Appendix D.

This page intentionally left blank.

2. APPROACH

This section describes the methodology for determining which observed aircraft tracks and encounters are considered littoral. The section subsequently discusses the selected procedure for quantitatively comparing the CONUS and littoral models and for determining that sufficient data were used to build the models.

2.1 LITTORAL SPATIAL FILTERING

The littoral environment is defined in Section 1.1 as the airspace extending from the coastline to international waters. Two slight modifications were made to this definition when filtering tracks and encounters for the models. First, a small buffer, corresponding to $1.67 \cdot 10^{-2}$ deg of latitude and longitude (approximately 1 NM) was added to the coastline in order to remove portions of tracks that transit small inlets (less than 2 NM wide) along the coast, including bays with small inlets—e.g., San Fransisco Bay. Second, no specific limit was placed in the distance from the coastline. Although no specific limit was placed on the distance from the coastline, there is a realistic limitation provided by the maximum range of the sensors. For long-range Air Route Surveillance Radars (ARSR-4) surrounding the edge of the CONUS, the maximum range specification for primary and secondary (beacon) surveillance is approximately 250 NM. Encounters have been observed out to approximately 450 NM at an altitude of 35,000 ft with secondary surveillance, although this relatively long 450 NM range does not extend to sea level.

The World Vector Shoreline Plus coastline product from the National Imagery and Mapping Agency was used to identify the coastline [16]. The highest resolution 1:250,000 scale source specification requires that 90 percent of all identifiable shoreline features be located within 500 meters. Oceanic islands, including the Caribbean islands, were classified as littoral. To create the buffer zone as described above, the 1:12,000,000 scale product was used to reduce computation time, and the buffer was created such that all coastal points were at least 1 NM from the buffer. An illustration of the coastline data with the buffer is shown in Figure 2. Once filtered with the littoral boundary, the remaining tracks are processed into the encounter models. Tracks with littoral duration less than 30 s were also removed from processing. After filtering, 10% of encounters and 3.8% of 1200-code flight hours passed the filter criteria—corresponding to 40,985 encounters and 2049 1200-code flight hours, respectively. Because of the relatively small data set used to build the littoral models when compared to the CONUS models, the question of whether adequate data were included within the model arises. It should be noted that although only 10% of encounters were classifed as littoral, these 40,985 encounters represent an order of magnitude increase in the number of encounter over previous models [17–22]. The process for determining this adequacy, in terms of the model convegerence, will be discused in the following section.

2.2 MODEL CONVERGENCE

After spatial filtering to determine which encounters and 1200-code tracks are in the littoral environment, the littoral models must make use of a significantly smaller data set than was used for
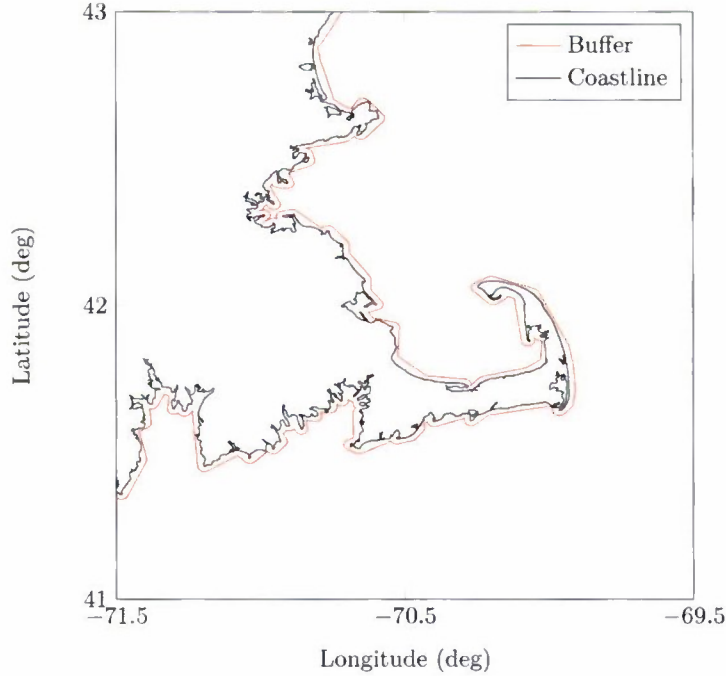
Figure 2. Littoral buffer for the Eastern Coast of Massachusetts. The littoral buffer was implemented to remove tracks transiting small coastal inlets and bays. The coastline is the 1:250,000 product while the buffer was created using the 1:12,000,000 scale product.

the CONUS models. Therefore, in addition to comparing the littoral and CONUS models to determine if they are similar, it must be determined that there are sufficient data in the littoral model. This is determined by comparing the convergence of (1) the parameters in the model and (2) the probability that an encounter leads to a near mid-air collision (NMAC) as data are added to the model. The $P(\text{nmac} \mid \text{enc})$ is the primary characteristic that is used to determine the effectiveness of a collision avoidance system using the encounter models, and it is therefore critical that this value converges.

In general, the convergence process is accomplished by adding fixed quantities of data (subsets of the total data set) and monitoring the convergence of the key parameters. There is not a quantitative metric for unequivocally concluding that the necessary metric converged. Thus, the convergence parameters are presented against those for the CONUS model and then discussed. This presentation of the convergence is sometimes termed the convergence curve. It is assumed that the parameters for the CONUS model converged, so direct comparison is made. The full data was split up into 32 approximately equal subsets for the convergence process. These individual subsets are denoted with superscript t while the cumulative sum of the data from the first subset through to subset t is denoted the (larger) data subset T.

2.2.1 Model Parameter Convergence

The first convergence metric is formed from the individual parameters that make up the Bayesian network—$\theta_{ijk} = P(X_i = k \mid \pi_{ij})$. Note that the nomenclature as defined in Appendix E is used

6

in this section. Using a metric that is dependent on the model parameters makes the metric independent of the model implementation—in this case, the simulation methodology. When these parameters converge, the many probability distributions that make up the model necessarily converge. The discrepancy between the parameters as additional data subsets are added is simply the difference between the parameters: $\theta_{ijk}^T - \theta_{ijk}^{T-1}$. Although this discrepancy may be used directly to determine the model convergence, there are instances when the discrepancy may be skewed. This occurs when the probability of a parental instantiation is low. For example, if a certain instantiation of the parents only occurs once in the data, then the change in the parameters given that instantiation would be large even though the probability of the parental instantiation is low. Hence, the joint probability of the variable and the parental instantiation, which weights each of the parameters by the probability of the parental instantiation, is used to determine convergence:

$$\phi_{ijk} = P(x_i, \pi_{ij}) = P(x_i \mid \pi_{ij})P(\pi_{ij}) = \frac{N_{ijk}}{N_i}, \tag{1}$$

where N_i is the number of data points for variable i. Note that the actual parameters of the model are computed by normalizing each individual count by the number of counts for each parental instantiation—N_{ijk}/N_{ij}. Since the models are composed of complete data (data without missing variables), then N_i is equivalent to the total number of data points (N) used for building the model. Since there are many parental instantiations, and thus many thousands of parameters, the mean of the difference between the joint probabilities is used as a summary statistic:

$$\delta\phi_T = \frac{1}{\sum_{i=1}^n r_i q_i} \sum_{ijk} |\phi_{ijk}^T - \phi_{ijk}^{T-1}|. \tag{2}$$

The joint probability discrepancy ($\phi_{ijk}^T - \phi_{ijk}^{T-1}$) will necessarily decrease as each equally sized subset is added because the ratio of the number of counts added at each iteration to the counts already in the model decreases as t increases. This effect will be illustrated using the following example. Suppose that there exists a model with one variable which can take on two values, A and B, and 400 data points exist for building the model. To determine convergence, the 400 points are separated into four equally sized subsets. Each subset has exactly 50 instantiations of A and 50 of B, although this is unknown a priori. In addition to computing the convergence parameters (ϕ_{ijk}) at each iteration, the maximum that each of these parameters can change given the data that are added at each iteration is also computed. This quantity is denoted $|\phi_{ijk,\max}^T - \phi_{ijk}^{T-1}|$, where $\phi_{ijk,\max}^T$ is the value that maximizes this quantity. This example is show in Table 1. As equal amounts of data are added (100 points), the maximum possible difference between the model parameters decreases from 0.25 to 0.13. To counteract this effect when adding equal quantities of data, Equation 2 is normalized by the mean of the maximum possible parameter discrepancy,

$$\delta\phi_{T,\max} = \frac{1}{\sum_{i=1}^n r_i q_i} \sum_{ijk} |\phi_{ijk,\max}^T - \phi_{ijk}^{T-1}|, \tag{3}$$

where the term $|\phi_{ijk,\max}^T - \phi_{ijk}^{T-1}|$ is defined as the maximum value that the joint probabilities can change given the parental instantiations that are observed with subset t. This maximum is found when

$$N_{ijk}^T = \begin{cases} N_{ijk}^{T-1} + N_{ij}^t & \text{when} \quad N_{ijk}^{T-1} = \min_{\pi_{ij}} N_{ijk}^{T-1} \\ 0 & \text{otherwise} \end{cases}, \tag{4}$$

TABLE 1

Example illustrating the maximum that the individual model parameters can change given that constant sized data subsets are added to the model.

T	N_A^T	N_B^T	ϕ_A^T	ϕ_B^T	$\phi_{A,\mathrm{max}}^T$	$\phi_{B,\mathrm{max}}^T$	$\lvert\phi_{A,\mathrm{max}}^T - \phi_A^{T-1}\rvert$	$\lvert\phi_{B,\mathrm{max}}^T - \phi_B^{T-1}\rvert$
1	50	50	0.5	0.5	-	-	-	-
2	100	100	0.5	0.5	0.75	0.25	0.25	0.25
3	150	150	0.5	0.5	0.67	0.33	0.17	0.17
4	200	200	0.5	0.5	0.63	0.38	0.13	0.13

where the quantity $\min_{\pi_{ij}} N_{ijk}^{T-1}$ is the minimum probability of the discrete distribution $P(x_i \mid \pi_{ij})$ for the data summation $T-1$. In other terms, this maximum value is found when all of the data for a parental instantiation at the current iteration is added to the parameter with the lowest value following the previous data iteration. This metric, $\delta\phi_T/\delta\phi_{T,\mathrm{max}}$, is termed the "normalized mean convergence", and qualitatively is a summary of how much the model parameters actually deviate compared to the maximum amount that the parameters can change. Considering only the error caused by sampling from the actual population of encounters, this metric is approximately constant over the number of iterations. When there are multiple disparate populations and one subset does not capture adequate samples from each population, then the metric will be observed to converge to a non-zero value with increasing data. The former behavior illustrates that an increased amount of data only reduces the error in estimating the discrete distributions, while the latter convergence behavior indicates that increased data also provide additional information. The normalized mean convergence will not converge to zero because the parameters in the model will almost always change due to sampling error when additional data are added.

2.2.2 NMAC Probability Convergence

The process for determining the $P(\mathrm{nmac} \mid \mathrm{enc})$ is different for the uncorrelated and correlated models. For the correlated model, the expected $P(\mathrm{nmac} \mid \mathrm{enc})$ is encoded directly in the model— $P(\mathrm{vmd} < 100\,\mathrm{ft}, \mathrm{hmd} < 500\,\mathrm{ft} \mid \mathrm{enc})$. When computing this probability, a uniform geographic assumption (over airspace class and altitude layer) was assumed to remove the effects of differing geographic distributions between the CONUS and littoral models (see Eq. 8). The $P(\mathrm{nmac} \mid \mathrm{enc})$ for the uncorrelated model must be determined through simulation since it is not explicitly defined within the model. Although simulation must be used to determine the NMAC probability, for the specific case of non-maneuvering aircraft (i.e., not accelerating, turning, or climbing), the $P(\mathrm{nmac} \mid \mathrm{enc})$ without a collision avoidance system is $r_{\mathrm{nmac}}^2/r_{\mathrm{enc}}^2$ when the ratio of cylinder height to width is the same for both the encounter cylinder and the NMAC cylinder. For the uncorrelated simulation, an encounter cylinder with a height of 2500 ft and a width of 12,500 ft was assumed (25 times the NMAC cylinder dimensions). Thus, the expected non-maneuvering NMAC probability is $1/25^2$ or $1.6 \cdot 10^{-3}$.

The direct sampling method for determining the NMAC probability convergence curve for the uncorrelated model would require simulating 32 sets of encounters, one for each addition of data.

In practice, upwards of one million encounters are required for each simulation, so the convergence determination process would required 32 million simulations. Instead, importance sampling [23] is used to reduce the computational requirement by creating one set of encounters for the model with the full data set and subsequently weighting the NMAC probability according the probability that the encounter would have resulted from each of the 32 submodels. The Bayesian network model, including the graphical structure (G) and the parameters (θ), is denoted B. B without a superscript denotes the model with the full set of data. The importance sampling procedure when determining the NMAC probability is estimated using

$$P(\text{nmac} \mid \text{enc}, B^T) = \frac{1}{N} \sum_i P(\text{nmac} \mid \text{enc}, B) \frac{P(\text{enc} \mid B^T)}{P(\text{enc} \mid B)} . \tag{5}$$

The term $P(\text{enc} \mid B^T)/P(\text{enc} \mid B)$ is termed the importance sampling weight and is

$$\frac{P(\text{enc} \mid B^T)}{P(\text{enc} \mid B)} = \frac{P(\mathbf{x}_1^{(i)} \mid B^T) P(\mathbf{x}_2^{(i)} \mid B^T)}{P(\mathbf{x}_1^{(i)} \mid B) P(\mathbf{x}_2^{(i)} \mid B)} , \tag{6}$$

where $\mathbf{x}_1^{(i)}$ and $\mathbf{x}_2^{(i)}$ are the model samples for encounter i and Aircraft 1 and Aircraft 2, respectively. $P(\mathbf{x}^{(i)})$ is the joint probability for the sample i from the posterior distribution of the encounter models (see Eq. E-1). The full formulation of $P(\mathbf{x}^{(i)})$ is the combination of the joint probabilities for the initial and transition Bayesian networks, although only the initial network is considered for this analysis. Ignoring the transition network is useful for numerical convenience, since considering the transition network after a few hundred time steps would make each probability computationaly inconsequential. Furthermore, the joint probability is only considered over the non-geographic bins to remove discrepancies in the probabilities caused by different geographical distributions. These assumptions result in $P(\mathbf{x}^{(i)})$ simplifying to $P(v^{(i)}, \dot{v}^{(i)}, \dot{h}^{(i)}, \dot{\psi}^{(i)})$, where the variables are defined at encounter initialization. It should be noted that the original method for initializing and weighting uncorrelated encounters to account for not using the appropriate sampling distributions (as in [7]) has been updated and is described in Appendix C. In addition to visually inspecting and discussing the results, the iteration where the NMAC probability estimate falls, and remains, within 1% and 5% of the final estimate is presented.

2.3 MODEL COMPARISON

One of the primary assumptions for forming separate littoral models is that the encounter characteristics are sufficiently dissimilar from the CONUS models to warrant using the separate models. Thus, an effort is undertaken in this section to develop a methodology to validate this assumption by first comparing the individual feature distributions, then the complete models themselves.

2.3.1 Marginal Distribution Comparison

A basic quantitative comparison between two discrete probability distributions is to directly compare the model's individual feature distributions—e.g., airspeed, vertical rate. Equation 7 displays

the method for computing the marginal distribution of the variable instantiation x_i given the conditional probability of the variable given the jth parental instantiation π_{ij} and the probability of the parental instantiation.

$$P(x_i) = \sum_{\pi_{ij}} P(X_i = k \mid \pi_{ij})P(\pi_{ij}) \tag{7}$$

It is possible that the marginal feature distributions for two regions may differ based solely on the different airspace structure—i.e., the airspace class (A) and altitude layer (L) distributions may vary, resulting in a perceived change in the overall aircraft behavior. For example, if the New York City airspace is compared to the North Dakota airspace, differences are expected in the feature distributions which is likely caused by differences in the airspace structure—the New York City airspace is saturated with terminal areas and a high aircraft density in Class A airspace while the North Dakota airspace is mostly Class E and G airspace below 18,000 ft mean sea level (MSL) with a small amount of transiting (en route) traffic. Thus, Equation 8 is used to remove this factor from the analysis, where $q_{A,L}$ is the number of A and L parental instantiations for variable i.

$$P_{\mathrm{obj}}(x_i) = \frac{1}{q_{A,L}} \sum_{A,L} P(x_i \mid A, L) \tag{8}$$

This formation essentially assumes an objective (uniform) probability distribution over A and L—the probability of each airspace class and altitude layer is assumed equal. An alternative is to assume the A and L distribution for one of the models although the metric as formulated ignores any dependence on these variables.

Classically, the Pearson's χ^2 goodness-of-fit test has been used to assess whether the difference between the expected and sampled univariate distributions is the result of sampling error [24]:

$$\chi^2 = \sum_{k=1}^{K} \frac{(n_{k,S} - n_{k,E})^2}{n_{k,E}}, \tag{9}$$

where K is the number of discrete bins, n_k is the kth bin frequency (counts), and the subscripts S and E denote the sampled and expected distributions, respectively. This formulation assumes that the χ^2 distribution has $K - 1$ degrees of freedom. For this discussion, the expected distribution will be that for the CONUS model while the sampled will be that of the littoral model. Using this formulation of the goodness-of-fit test assesses the null hypothesis that the difference between the expected distribution (CONUS) and sampled distribution (littoral) is caused by sampling error alone. This test was originally intended for relatively small sample sizes: as the number of samples increases beyond approximately 10,000, χ^2 becomes highly sensitive to minor deviations between the two distributions such that the deviations may become statistically significant according to the test [25]. To illustrate this effect and the amount of deviation that the test allows, Equation 9 is solved for the deviance, defined according to

$$d(\chi^2) = |p_S - p_E| = \sqrt{\frac{\chi^2}{nK^2}}, \tag{10}$$

where p is the bin frequency (n_k) normalized by the sample size n. The deviance is defined as the assumed constant relative frequency difference between the expected and sampled distributions

when the expected distribution (p_E) is assumed uniform. The subscript k is excluded in Equation 10 to stress that the deviance assumes that the difference between each frequency is constant for each bin. Furthermore, this metric should not be confused with the expected value of the bin frequency difference. Although $d(\chi^2)$ provides insight into the χ^2 test's allowable difference between the distributions, Equation 9 is again modified, this time assuming that the total difference between distributions is associated with a single bin. Although this is not practically possible since the relative frequencies (p) must sum to unity for each distribution, this formulation of the deviance places an upper bound on the allowable difference for each bin. This formulation is termed the maximum deviance, and is given by

$$d_{\max}(\chi^2) = \sqrt{\frac{\chi^2}{nK}} \geq \arg\max(|p_{k,S} - p_{k,E}|). \tag{11}$$

Observe that the constructions for $d(\chi^2)$ and $d_{\max}(\chi^2)$ differ by $\sqrt{1/K}$. This definition of the deviance should not be confused with the Bayesian deviance which is also used to compare the fit of probabilistic models [26]. For a sample size of 10,000, assuming a p-value of 5%, with seven bins, $d(\chi^2) = 5.1 \cdot 10^{-3}$ and $d_{\max}(\chi^2) = 1.34 \cdot 10^{-2}$, indicating that very small deviances would result in rejecting the hypothesis that the distributions were equivalent. Hamada et al. [27] recommend selecting the number of bins proporational to the sample size, or $K \approx n^{0.4}$, when using a goodness-of-fit test. Since the bins are already defined for the encounter models, the sample size used for calculation of the χ^2 statistic may be modified, resulting in a goodness-of-fit test of the formulation

$$\chi^2 = n_m \sum_{k=1}^{K} \frac{(p_{k,S} - p_{k,E})^2}{p_{k,E}}, \tag{12}$$

where n_m is the modified sample size ($n_m = K^{2.5}$ according to Hamada et al.). The deviance and maximum deviance for $n_m = K^{2.5}$ and $n_m = 1000$ as a function of the number of bins are shown in Figure 3 to illustrate the difference between the two effective sample size assumptions.

Since the CONUS and littoral models are compared directly, the true sample size of the marginal littoral distribution is the number of data points filtered by the littoral buffer ($7.38 \cdot 10^6$). The standard χ^2 test would almost certainly reject the two distributions as being equivalent due to the large number of data instances; therefore, the modified sample size n_m is instead set to 1000. This is equivalent to allowing the same distribution discrepancy that is accepted for the standard χ^2 test with 1000 samples. Using the χ^2 test with a modified sample size of 1000, allows for deviances caused by factors other than sampling error. The sample size formulation proportional to K is not used since it allows an unacceptable deviance with fewer than five bins. Because the results of any hypothesis test may be misleading, the associated p-values and the distributions themselves are also presented. The p-value is the probability of obtaining the sample (littoral) distribution or one more extreme by chance alone; thus, a p-value near zero indicates little confidence that that the sample came from the proposed distribution.

2.3.2 Bayesian Network Similarity Score

Although comparing the marginal feature distributions provides a quantitative measure of the discrepancy between the two distributions, it does not consider the interdependences between variables
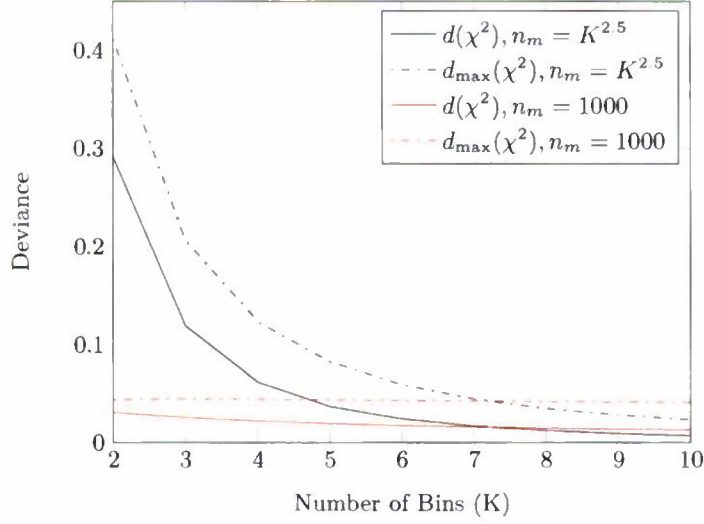
Figure 3. Deviance metric sensitivity to number of bins assuming a p-value of 5%. Shown is the the nominal and maximum deviance for two definitions of the sample size.

that are explicitly captured within the Bayesian network. A complete comparison between the two models should consider this important model characteristic. In order to quantitatively compare the models, the probability that two different populations have the same Bayesian network parameters given the recorded data is computed. This assumes that the graphical structure of both networks is identical.

The true parameters of the two populations are denoted as θ_1 and θ_2 and the data associated with the two populations as D_1 and D_2. The posterior is computed as $P(\theta_1 = \theta_2 \mid D_1, D_2)$, which involves multiplying the prior distribution of the hypothesis that $P(\theta_1 = \theta_2)$ by the ratio

$$\frac{P(D_1, D_2 \mid \theta_1 = \theta_2)}{P(D_1, D_2)} = \frac{\int P(D_1, D_2 \mid \theta)p(\theta)\,d\theta}{\left[\int P(D_1 \mid \theta)p(\theta)\,d\theta\right]\left[\int P(D_2 \mid \theta)p(\theta)\,d\theta\right]}\,. \tag{13}$$

Defining $f(D) = \int P(D|\theta)p(\theta)\,d\theta$, the ratio becomes

$$\frac{f(D_1 \cup D_2)}{f(D_1)f(D_2)}\,. \tag{14}$$

As shown by Cooper and Herskovits [28] and using the notation used in Appendix E,

$$f(D) = \prod_{i=1}^{n} \prod_{j=1}^{q_i} \frac{\Gamma(\alpha_{ij0})}{\Gamma(\alpha_{ij0} + N_{ij})} \prod_{k=1}^{r_i} \frac{\Gamma(\alpha_{ijk} + N_{ijk})}{\Gamma(\alpha_{ijk})}\,, \tag{15}$$

where α is the prior and Γ is the standard gamma function. The natural logarithm of the ratio in Equation 13 is used to compare the feature distributions from the different data sets. The more positive the log-ratio is, the more likely the distributions are the same. Negative log-ratios indicate that the distributions are different. Because this metric is not intuitive, the maximum log-ratios are also presented; this maximum is simply the CONUS model compared against itself. Positive log-ratios near this maximum indicate greater similarity than positive log-ratios near to zero.

3.   UNCORRELATED ENCOUNTER MODEL

Figures 4 and 5 illustrate the optimal initial and transition network structures for the littoral uncorrelated model, respectively. Note that the optimal littoral initial network is identical to that for the CONUS model while the transition networks differ (see Appendix D.1 for the network candidates considered). The sole difference is that the initial airspeed (v) is not a parent variable in the littoral transition network. This reduces the transition network complexity such than the number of parameters is reduced from 22,344 for the CONUS model to 6972 for the littoral model.
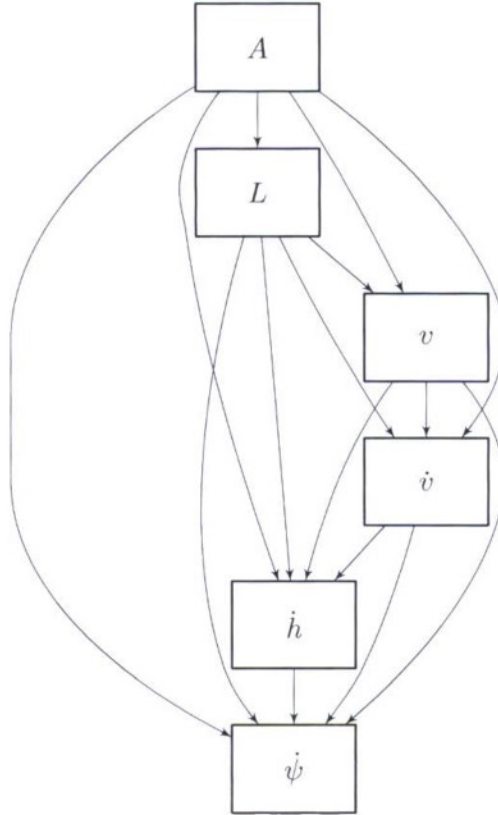

Figure 4. Bayesian network structure representing the initial conditions for the littoral uncorrelated model.

3.1   CONVERGENCE

The model parameter convergence as discussed in Section 2.2.1 for the initial network structure is shown in Figure 6. Both the CONUS and littoral models display approximately the same general behavior, although for all iterations, the normalized mean convergence is lower for the CONUS model. This is expected due to the significantly larger amount of data available for the CONUS
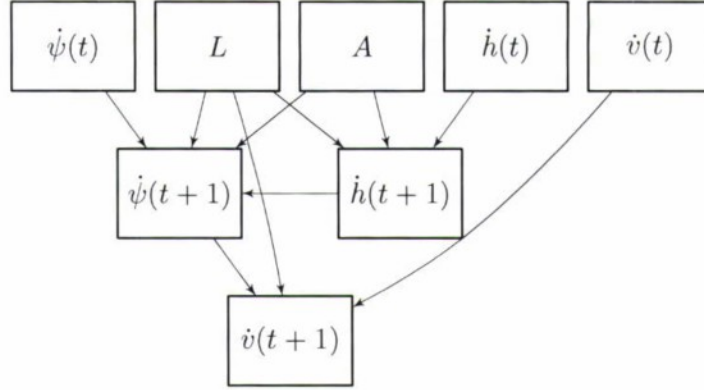
Figure 5. Transition network structure for the littoral uncorrelated model. The transition network propagates the initial conditions during the encounter and is updated at one second intervals.

model which results in a reduced sampling error. Because of the similar behavior (the same observed ratio between the littoral and CONUS values), the mean of the ratio between the two mean convergence is computed. This results in an estimate of the relative convergence between the two models. The mean of the ratios between the CONUS and littoral convergences shown in this figure is 3.83, indicating that the littoral model parameters converged to about 26% of that for the CONUS model.
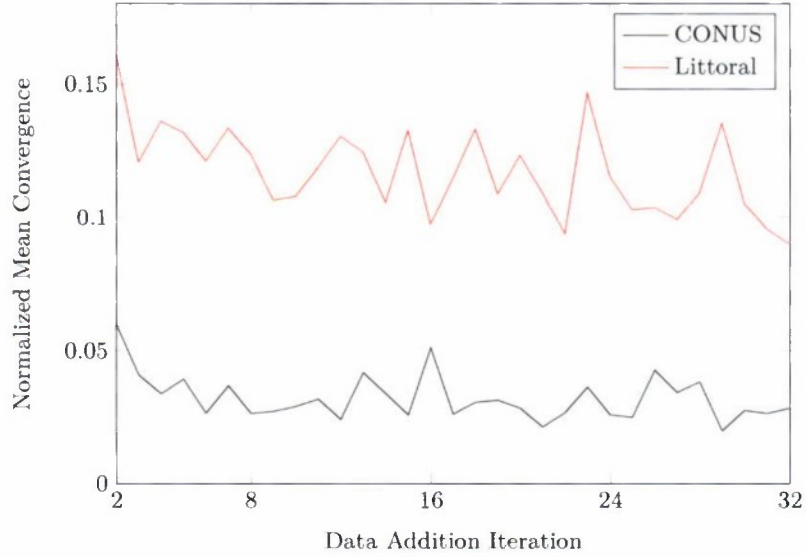

Figure 6. Uncorrelated model initial parameter convergence for the CONUS and littoral models.

Figure 7 shows the normalized mean convergence for the transition network. The mean of the ratios between the two models is reduced from 3.82 for the initial network to 2.39 for the transition net-

14

work. This slight reduction is caused by an associated reduction in the total number of parameters that must be estimated in the littoral transition network.
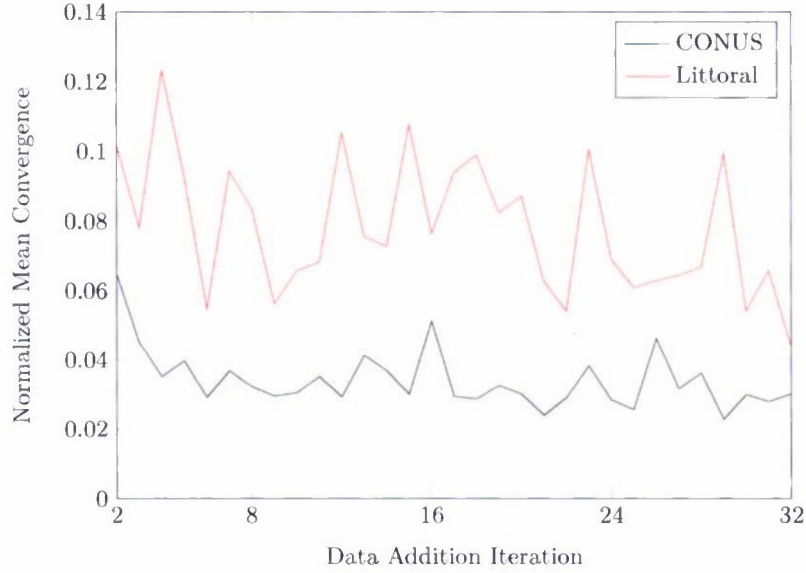

Figure 7. Uncorrelated model transition network parameter convergence for the CONUS and littoral models.

From these two convergence illustrations, there is an observed relationship between the normalized mean convergence and the total number of estimated parameters together with the number of observations used to build the model. This relationship, the mean ratio between the normalized mean convergences for the CONUS and littoral models, is observed to be approximately

$$\zeta \left(\frac{N_{\text{conus}} n_{\text{littoral}}}{N_{\text{littoral}} n_{\text{conus}}} \right)^{1/2} , \tag{16}$$

where N is the total number of observations (equivalent to N_i for a model without missing data), n is the the total number of parameters in the model, and ζ is a correction constant. This correction factor is introduced because the expression does not consider the complex model interdependences and how the data affects the selection of the optimal network. From the data, ζ is 1.34 for the initial network and 1.2 for the transition network, indicating strong confidence in this relationship between the convergence metric and model's number of parameters and observations.

Although the normalized mean convergence allows for the quantitative comparison between the parameter convergence of the two models, the $P(\text{nmac} \mid \text{enc})$ convergence provides a metric which demonstrates how the quantity of data together with the optimal network structure will affect the specific quantity of interest. This $P(\text{nmac} \mid \text{enc})$ estimate using the procedure discussed in Section 2.2.2 for both the CONUS and the littoral models is shown in Figure 8. From visual inspection, it was determined that the CONUS model converged at approximately 18 iterations, while the littoral model converged at 26 iterations. This aligns with the 1% threshold when assessing

15

the percent deviation from the final $P(\text{nmac} \mid \text{enc})$ estimate—both the littoral and CONUS model converged to within 1% at 18 iterations. The CONUS model converged to within 5% of the final estimate immediately (at the first iteration) while the littoral model converged at iteration 12. The theoretical $P(\text{nmac} \mid \text{enc})$ should be $1.6 \cdot 10^{-3}$ under the assumptions presented in Section 2.2.2. The $P(\text{nmac} \mid \text{enc})$ in the figure may not exactly match because of sampling error, and the model characteristics (e.g., acceleration, turn rates) that were not considered in the extensive assumptions used for the $1.6 \cdot 10^{-3}$ approximation.
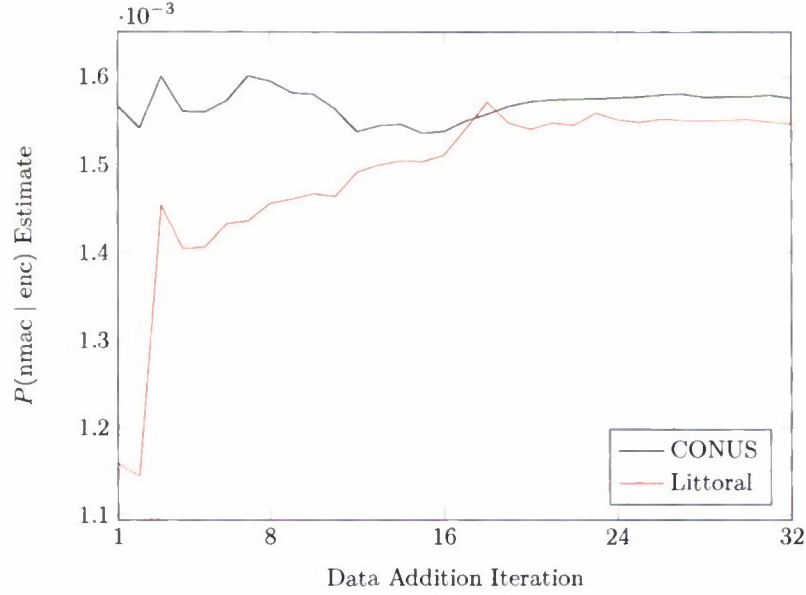

Figure 8. Uncorrelated P(nmac | enc) convergence for the CONUS and littoral models.

3.2 MODEL COMPARISON

Figure 9 illustrates the comparison of the marginal discrete distributions for the model variables. Superimposed is the p-value calculated from Equation 12 using the standard χ^2 probability distribution with $K - 1$ degrees of freedom. The p-value is the probability of obtaining the sample (littoral) distribution or one more extreme by chance alone; a p-value near zero indicates little confidence that the two distributions are equivalent. The marginal distributions for the non-geographic variables, including airspeed, acceleration, vertical rate, and turn rate, were marginalized assuming an objective (uniform) distribution over airspace class and layer (Eq. 8) while airspace class and altitude layer distributions are the standard marginal distributions (Eq. 7).

The p-value results for airspace class, vertical rate, and acceleration are close to but below the commonly used 1% threshold. This indicates that the distributions are not equivalent according to the threshold, but the deviances observed for these variables are relatively minor compared to the airspeed and altitude layer deviances. The hypothesis tests for airspeed, altitude layer and turn
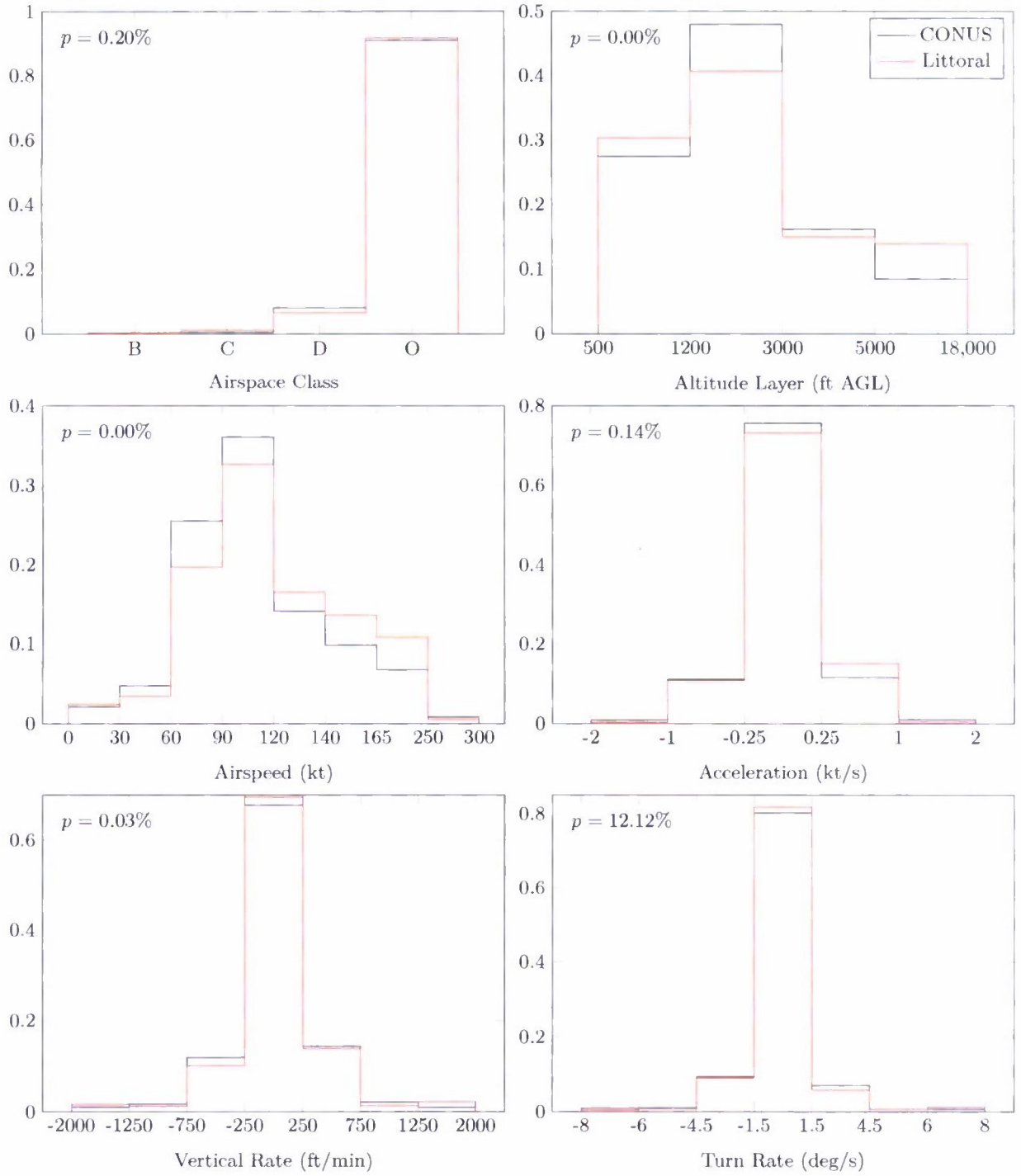
16

Figure 9. Uncorrelated relative frequency feature comparison with the modified χ^2 p-value superimposed, denoted p (Eq. 12).

rate demonstrate the results with high confidence, defined as a p-value very near zero or greater than 10%. The test indicates that the turn rate distributions are equivalent while the airspeed and altitude layer distributions are different. In general, the marginal distribution comparision illustrates that littoral 1200-code aircraft have higher airspeeds and travel at higher altitudes than their CONUS equivalent.

Table 2 shows the Bayesian network similarity score for the initial and transition networks. Also shown is the maximum possible value which is found by comparing the CONUS model to itself. Unfortunately, this metric can only be computed when the network structures are the same for both of the models being compared. The optimal transition network structures are different for the CONUS and littoral models, thus the littoral transition network was formed to match that for the CONUS model. This test, discussed in Section 2.3.2, indicates that the initial network parameters are different between the models with very high confidence, but that the transition networks are similar. From Figure 9, the littoral altitude layer distribution was statistically different than for the CONUS model. Therefore, the Bayesian similarity score test was also performed for each instantiation of altitude layer and airspace class, 16 in total, and consistent results to those in Table 2 were observed for each instantiation—all initial network similarity scores were negative while all transition network scores were positive.

TABLE 2

Uncorrelated model similarity scores.

Network	Score	Maximum Score
Initial	−959,784	70,831
Transition	41,117	86,122

4. CORRELATED ENCOUNTER MODEL

Figures 10 and 11 show the optimal initial and transition network structures for the littoral correlated model, respectively. Similar to the littoral uncorrelated model, the optimal initial network is the same for the CONUS and littoral models while the optimal transition networks differ (see Appendix D.2 for the network candidates considered). The altitude layer variable (L) is not a parent variable in the littoral correlated transition network while it is in the CONUS model. The absence of the altitude layer as a parent variable reduced the number of parameters in the transition network from 8100 for the CONUS model to 324 for the littoral model, a 25 fold reduction.
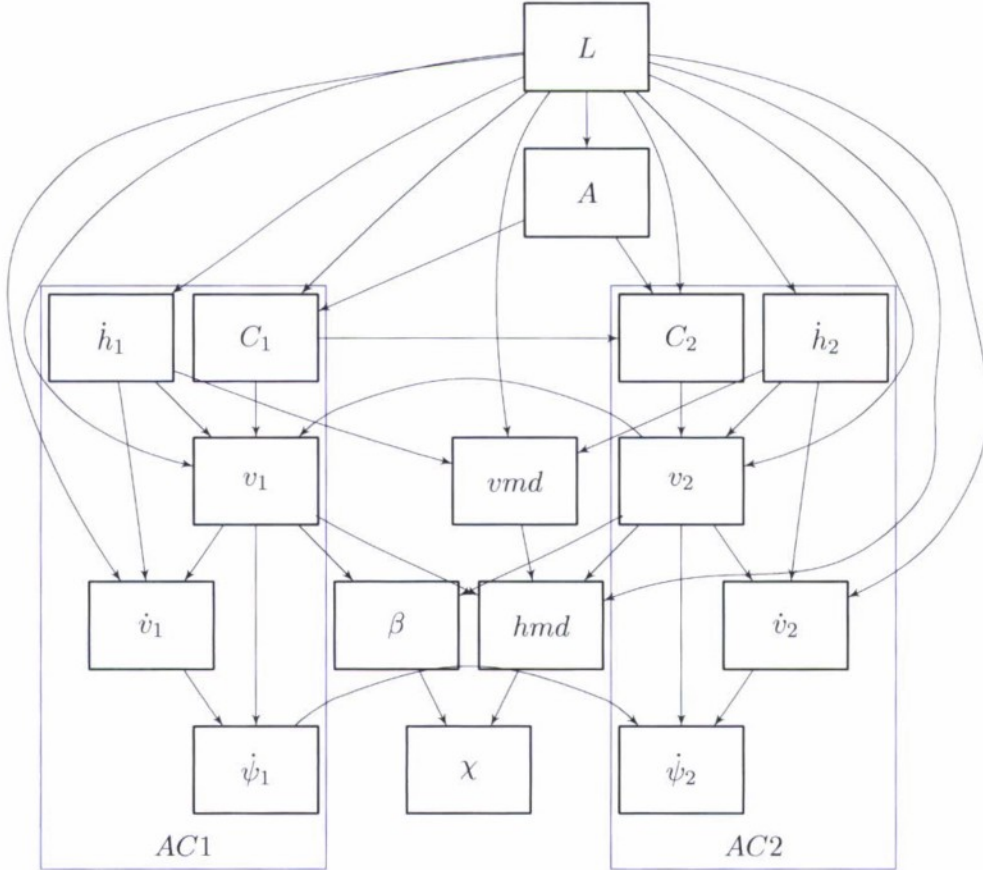

Figure 10. Bayesian network structure representing the initial conditions for the littoral correlated model.

4.1 CONVERGENCE

Figure 12 illustrates the normalized mean convergence for the initial network. The mean ratio of the normalized mean convergence for the littoral model normalized by that for the CONUS model was 2.99, indicating that the littoral model converged to 33% of that for the CONUS model. The
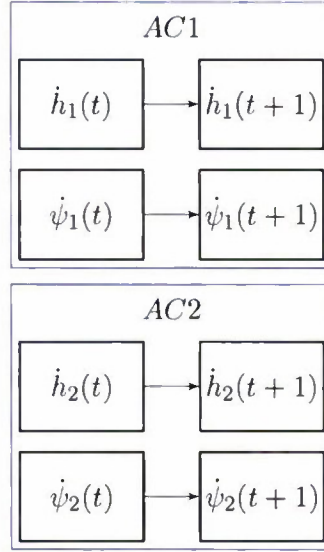
Figure 11. Transition network structure for the littoral correlated model.

relationship of Equation 16 was found to be equally valid for the correlated initial network, with ζ being 1.06. The normalized mean convergence in Figure 12 demonstrates convergence behavior, as opposed to remaining constant, indicating that the individual data subsets do not encompass the complete diversity of encounters. Hence, several iterations are required before the normalized mean convergence metric approaches steady state.
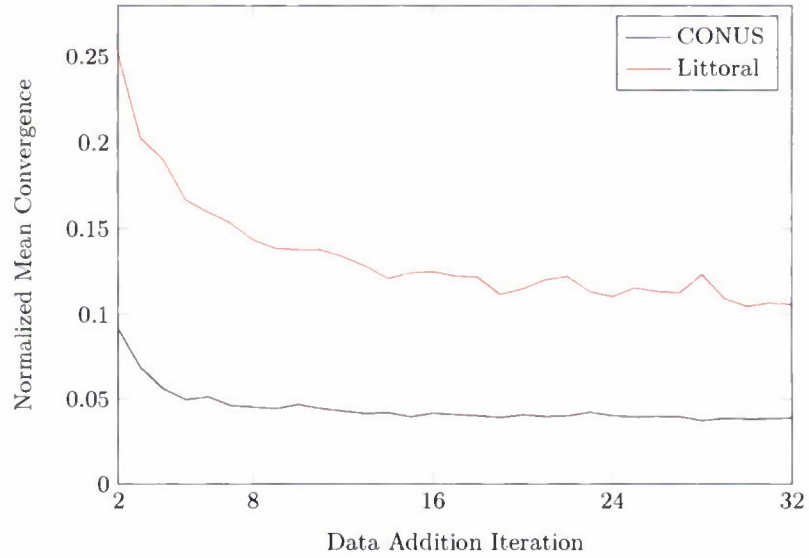

Figure 12. Correlated model initial parameter convergence for the CONUS and littoral models.

Figure 13 illustrates the convergence for the transition network. Contrary to the convergence for the previous networks discussed, the normalized mean convergence is lower in general for the littoral model relative to the CONUS model. This is indicated by the mean ratio of the normalized convergence being 0.93 while it was greater than two for the other comparisons. This behavior is caused by the littoral correlated transition network having 25 times fewer parameters than the CONUS network while approximately 10% of the CONUS data was used for the littoral model. The correction factor ζ for this case was 0.69, which is lower than that for the other convergence curves. This result indicates that Equation 16 with ζ set to unity is only an approximation of the benefit of adding data to the encounter models using the normalized mean convergence metric.
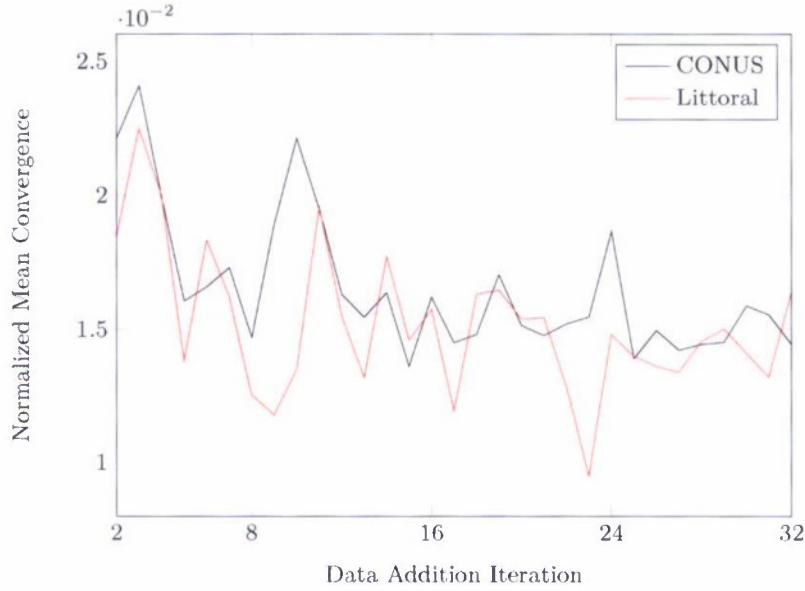

Figure 13. Correlated model transition network parameter convergence for the CONUS and littoral models.

Although there is confidence that the littoral transition network parameters converged, there is still interest in the $P(\text{nmac} \mid \text{enc})$ convergence. Similar to the discrete marginal distribution comparison, a uniform marginalization over A and L was assumed to remove the effects of differing geographic distributions. This is illustrated in Figure 14. The CONUS model was determined (by visual inspection) to converge quite quickly, after about 12 iterations, while the NMAC probability for the littoral model was determined to converge after about 28 iterations.

The convergence curve's percent deviation from the final $P(\text{nmac} \mid \text{enc})$ is illustrated in Figure 15. The littoral and CONUS model convergence falls within the 5% threshold at 31 and 20 iterations, respectively, while neither model's convergence falls and remains within the 1% threshold. The littoral model would converge to below 5% at 27 iterations, but the percent deviation increases to 5.5% at iteration 30. The result that the models do not converge to within 1% indicates that this arbitrary convergence threshold cannot be used independant of the general convergence behavior since it was assumed that the CONUS model converged.
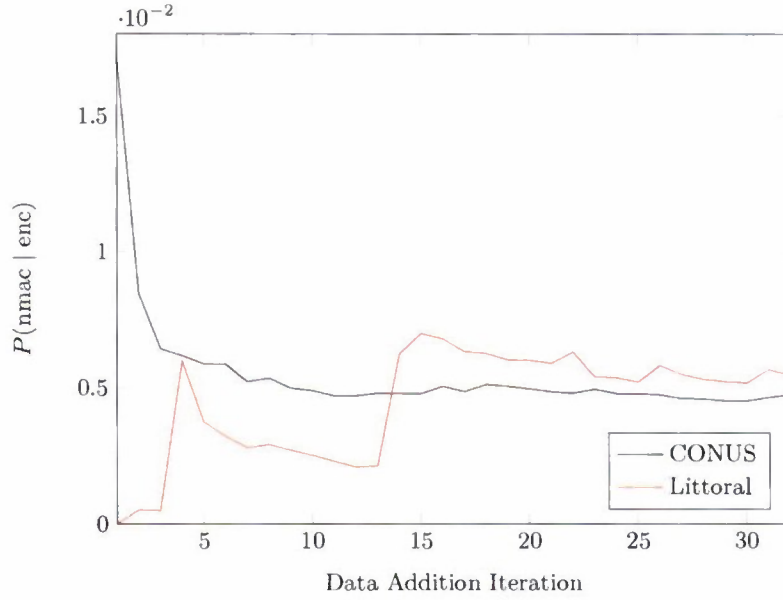
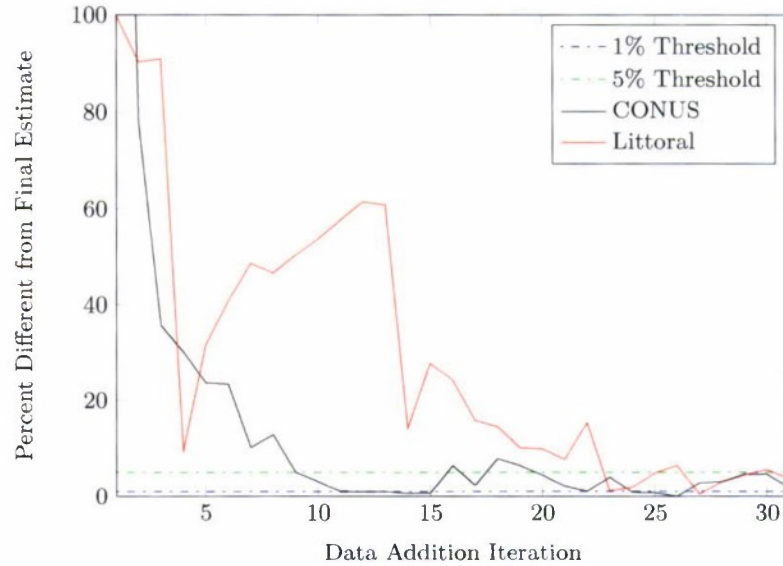*Figure 14. Correlated P(nmac | enc) convergence for the CONUS and littoral models.*

Figure 15. Correlated P(nmac | enc) convergence expressed as the difference from the final estimate. The absolute value is presented, and the percent deviation is truncated at 100%. Doing so removes the CONUS model's first iteration point which is at approximately 250%.

4.2 MODEL COMPARISON

Similar the the comparison process for the uncorrelated model, the marginal distributions for the variables in the initial network are first compared, followed by the Bayesian network similarity score. For the purpose of the marginal comparison, the variables for both aircraft were combined

into one marginal distribution. The geographic variables, along with the airspeed, acceleration, vertical rate, and turn rate are shown in Figure 16. The geographic variables (i.e., altitude layer and airspace class) were determined to have different distributions with high confidence while the other variables were determined to have similar distributions. The airspeed distribution has the largest discrepancy of these non-geographic variables, which is indicated by the relatively low p-value. In general, it was observed that more littoral encounters occur in the lower altitude band, and that aircraft in littoral encounters tend to have lower vertical rates and turn rates when compared with CONUS encounters.

Figure 17 illustrates the marginal comparison for the variables that are defined at the closest point of approach—termed the geometric variables. The hypothesis test indicates that all of the feature distributions are nearly the same, except for the the approach angle distribution. The aircraft category hypothesis test indicates that the distributions are not equivalent, but only nearly so with a p-value of 0.99%.

Table 3 shows the Bayesian similarity scores. Both the initial and transition networks for the littoral model were determined to be similar to the CONUS model although the littoral transition network corresponded better to the CONUS model than did the initial network. Similar to the methodology for the uncorrelated model, the individual parental instantiations were also compared. The CONUS and littoral models agreed (all log-ratios were positive) except for the single instantiation of airspace classified as "other" and the lower altitude layer for the initial network. This instance may be caused by differing airspace procedures over the oceanic airspace at lower altitudes away from terminal areas.

TABLE 3

Correlated model similarity scores.

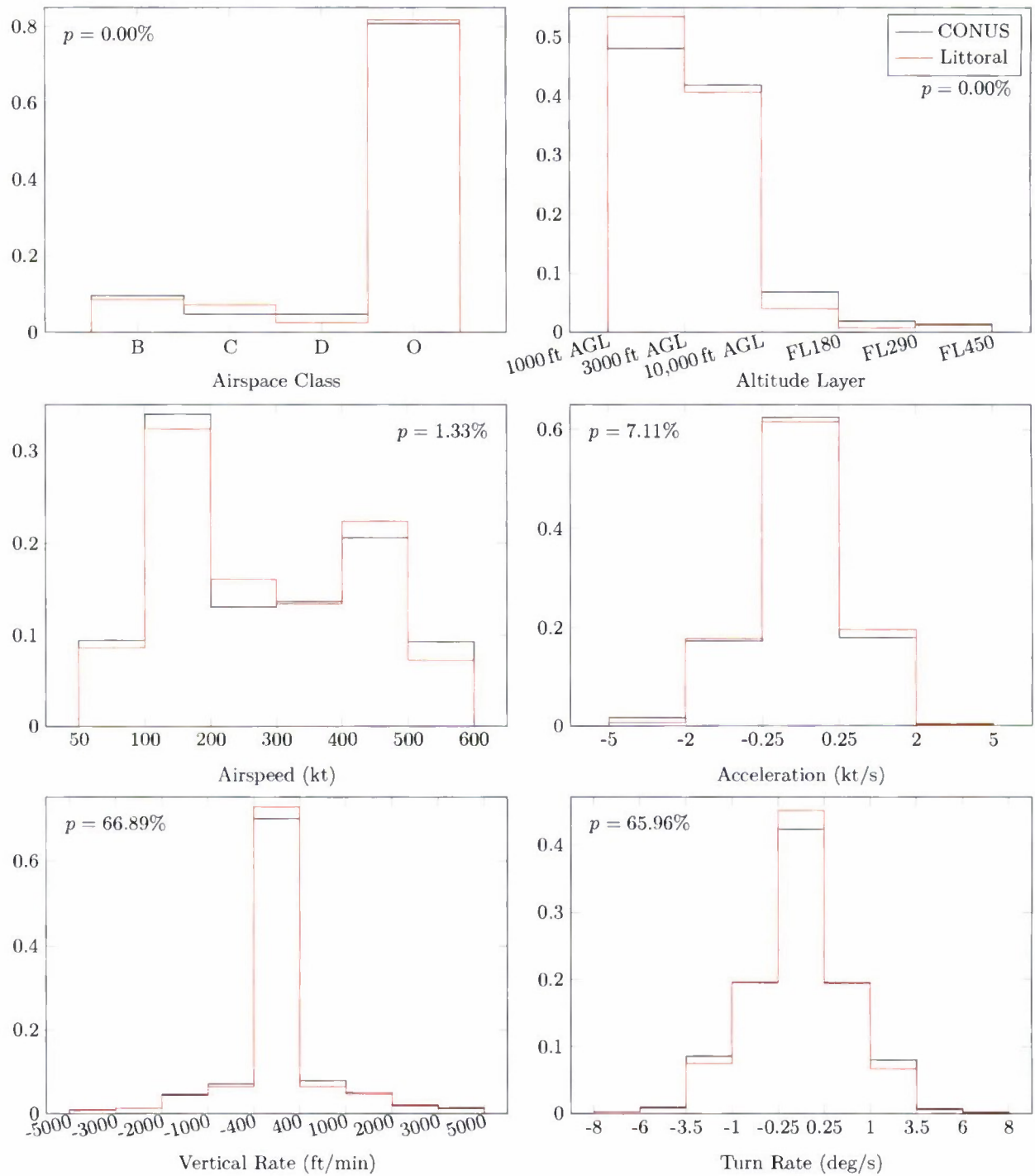| Network	Score	Maximum Score
Initial	1705	20,413
Transition	20,910	36,467

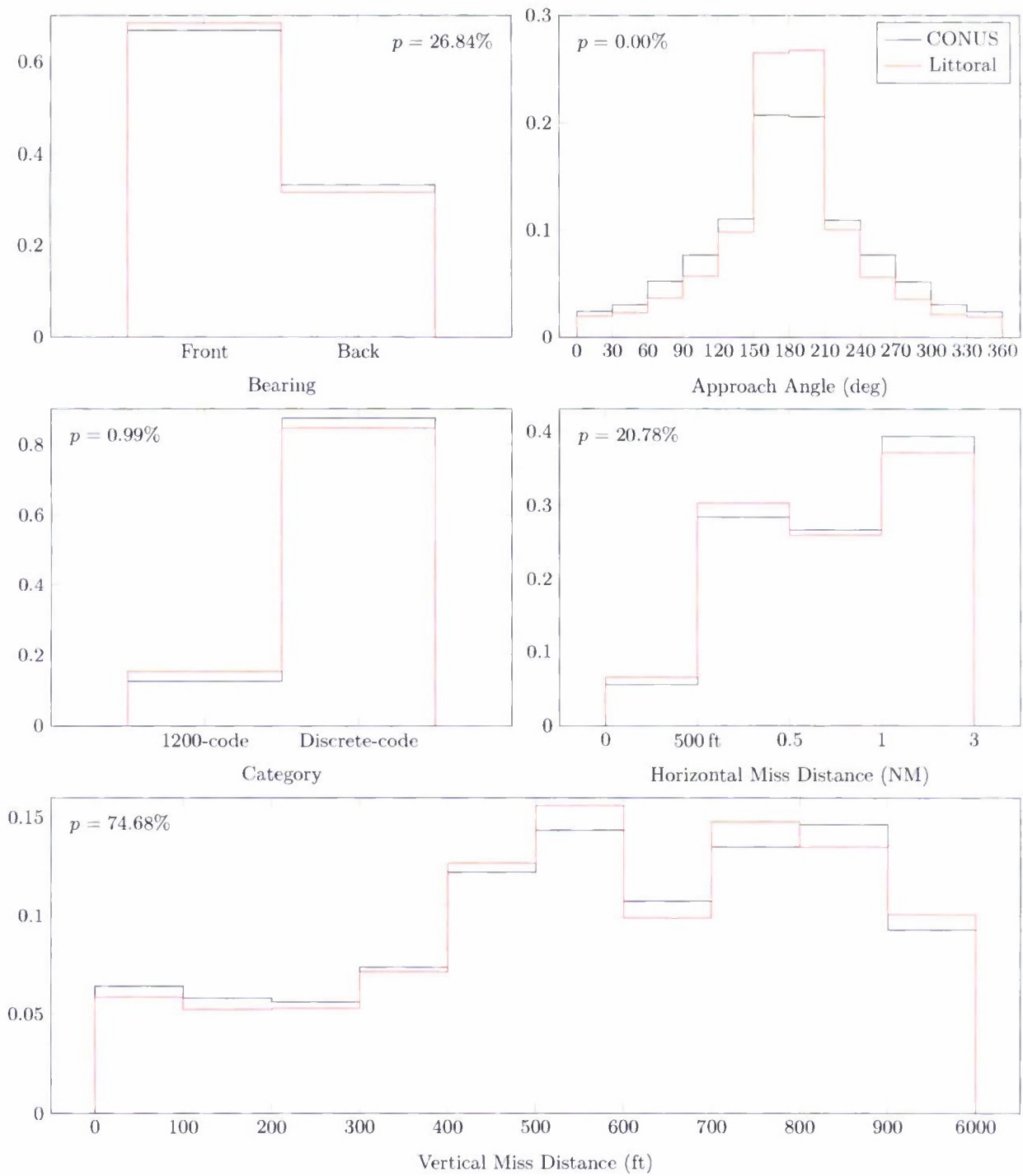*Figure 16. Correlated relative frequency feature comparison.*

Figure 17. Correlated relative frequency feature variable comparison for variables defined at CPA.

This page intentionally left blank.

5. SUMMARY

The purpose of this analysis was to build a correlated and an uncorrelated conventional encounter model for the littoral regions of the National Airspace System. Recently, an exhaustive set of encounter models was built for the continental United States, encompassing conventional and unconventional aircraft in correlated and uncorrelated encounters. Although these CONUS models captured encounters in the littoral region surrounding the CONUS, they did not explicitly classify the encounters into the littoral and non-littoral regions. Hence, the nine months of radar data used to build the original models were filtered to build these models specific to the littoral region. A littoral unconventional model was not built because of the very low occurrence of aircraft classified as unconventional (e.g., gliders, balloons) that were observed in the littoral airspace.

The littoral region was broadly defined as the region where a maritime UAS would be likely to operate. Specifically, the littoral region was defined with respect to the shoreline, and an additional buffer of approximately 1 NM was added oceanward to remove any traffic that may be identified as littoral when transiting small oceanic inlets or bays. After filtering, fewer than 10% of the data were determined to be oceanic—10% of encounters and 3.8% of 1200-code track data were appropriate for building the correlated and uncorrelated models, respectively. Because of this relatively small quantity of data, one of the primary concerns was the convergence of the model. In addition, the CONUS and littoral models were directly compared to ensure that the littoral and CONUS models were statistically and realistically different.

In order to determine if the models converged, two metrics were formed. First, the change in the model parameters as data were added was assessed. Second, the primary safety analysis metric of interest—$P(\text{nmac} \mid \text{enc})$—was estimated as addition data were added. These convergence metrics were directly compared to those of the CONUS models. To determine whether the models were equivalent, the marginal discrete feature distributions were compared using a modified χ^2 similarity metric. Since this test was not able to capture the important dependencies in the Bayesian network models, the littoral and CONUS model were also compared using what was termed the Bayesian network similarity score which directly compared the model parameters.

The primary conclusions of this work were:

1. Both the littoral uncorrelated and correlated models converged. This was determined primarily through analysis of the $P(\text{nmac} \mid \text{enc})$ as additional data were added since in all but one case, the littoral model parameters did not converge to the level of the CONUS model. In the other case, the littoral model converged to a greater extent because there were 25 times fewer parameters to be estimated in the littoral optimal model than for the CONUS optimal model. For both the correlated and uncorrelated models, the $P(\text{nmac} \mid \text{enc})$ converged much faster for the CONUS model. The CONUS model required 18 and 12 of the 32 iterations to converge for the uncorrelated and correlated model, respectively, while the littoral model required 26 and 28 iterations, respectively.

2. It was determined that neither littoral model was significantly similar to its CONUS counterpart to warrant not using the littoral models.

(a) For the uncorrelated models, the littoral initial network was found to be significantly dissimilar from the CONUS initial network when using both the marginal distribution test and the Bayesian network similarity score. Specifically, the airspeed and altitude layer distribution varied greatly between the littoral and CONUS uncorrelated initial networks. The littoral and CONUS correlated model initial networks were found to be similar using the Bayesian network similarity score, although the geographic variables (airspace class and altitude layer) and the approach angle at closest point of approach (CPA) were found to be dissimilar.

(b) The transition networks for both the littoral correlated and uncorrelated models were found to be similar to the CONUS models using the Bayesian network similarity score. This was true even though the optimal littoral transition network was not used because the scoring metric required the same network structure for the models being compared. For both the correlated and uncorrelated models, the littoral and CONUS initial networks were found to be less similar than the transition networks. This discrepancy is thought to be caused by underlying differences in the airspace affecting the initial network, while the pilot's behavior, which would affect the transition network, remains similar.

5.1 FUTURE WORK

A comprehensive safety analysis requires the characterization of both the encounter attributes (as was accomplished in this document) as well as the airspace density. The NMAC rate in a given airspace is the combination of the expected encounter rate and the probability that an encounter event leads to a NMAC. The expected encounter rate is directly proportional to the average airspace density.

It is not trivial to characterize the noncooperative traffic density because primary radar returns consist of clutter and birds in addition to the noncooperative traffic of interest. Furthermore, many ATC radars cannot estimate altitude (other than ARSR-4 sensors on the exterior of the CONUS), so either altitude cannot be considered or it must be estimated using a technique called multiangulation. Lincoln Laboratory has completed a preliminary study classifying noncooperative tracks into birds and aircraft [29] and has also developed preliminary algorithms for multiangulation using a network of two-dimensional ATC radars [30]. It is therefore recommended that a methodology for characterizing the littoral noncooperative density be established.

Encounter characteristics and traffic density are expected to change as the Federal Aviation Administration implements the Next Generation Air Transportation System (NextGen), commercial air traffic density increases, and newer vehicles are introduced into the NAS (e.g., UASs, very-light jets). It is important that the encounter and airspace density models are kept current throughout the development and certification of the UAS SAA systems. This ensures that conclusions derived from the models are valid when the system reaches initial operating capability. This process includes capturing recent airspace data, monitoring the airspace characteristics for changes, and updating the encounter models as necessary.

The DHS UAS operational environment may extend beyond the limits of CONUS-based ground radars. Therefore, it is important to characterize the oceanic environment beyond the range of these sensors—e.g., the Carribean Sea, northern coast of South America. Data sources and a methodology for utilizing these sensors should be established to create encounter and density models representative of the expected oceanic operating environment.

This page intentionally left blank.

APPENDIX A
CONTINUOUS FEATURE COMPARISON

The following sections display the continuous model feature distributions that were discretized when building the models (except for variables that are fundamentally discrete, such as airspace class). The distributions are normalized such that the integral over the feature limits for both the CONUS and littoral models are equal.

A.1 UNCORRELATED MODEL
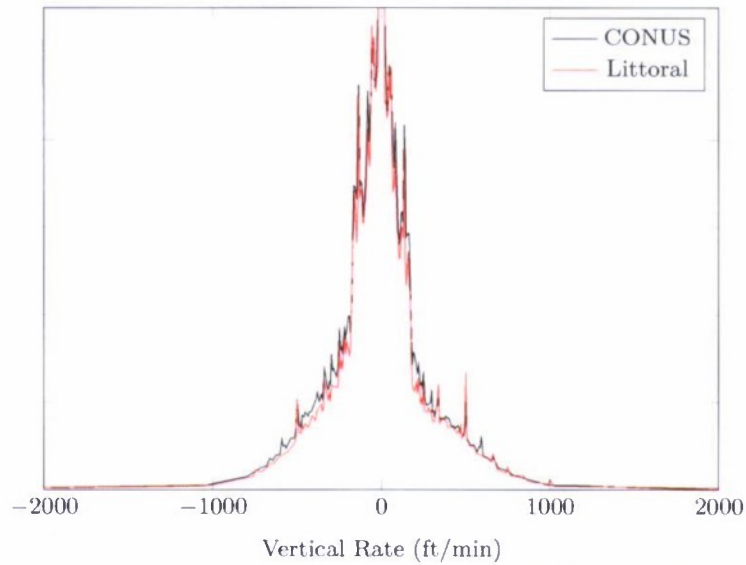
Figure A-1. Aircraft vertical rate in uncorrelated encounters magnified for detailed view of distribution tails.
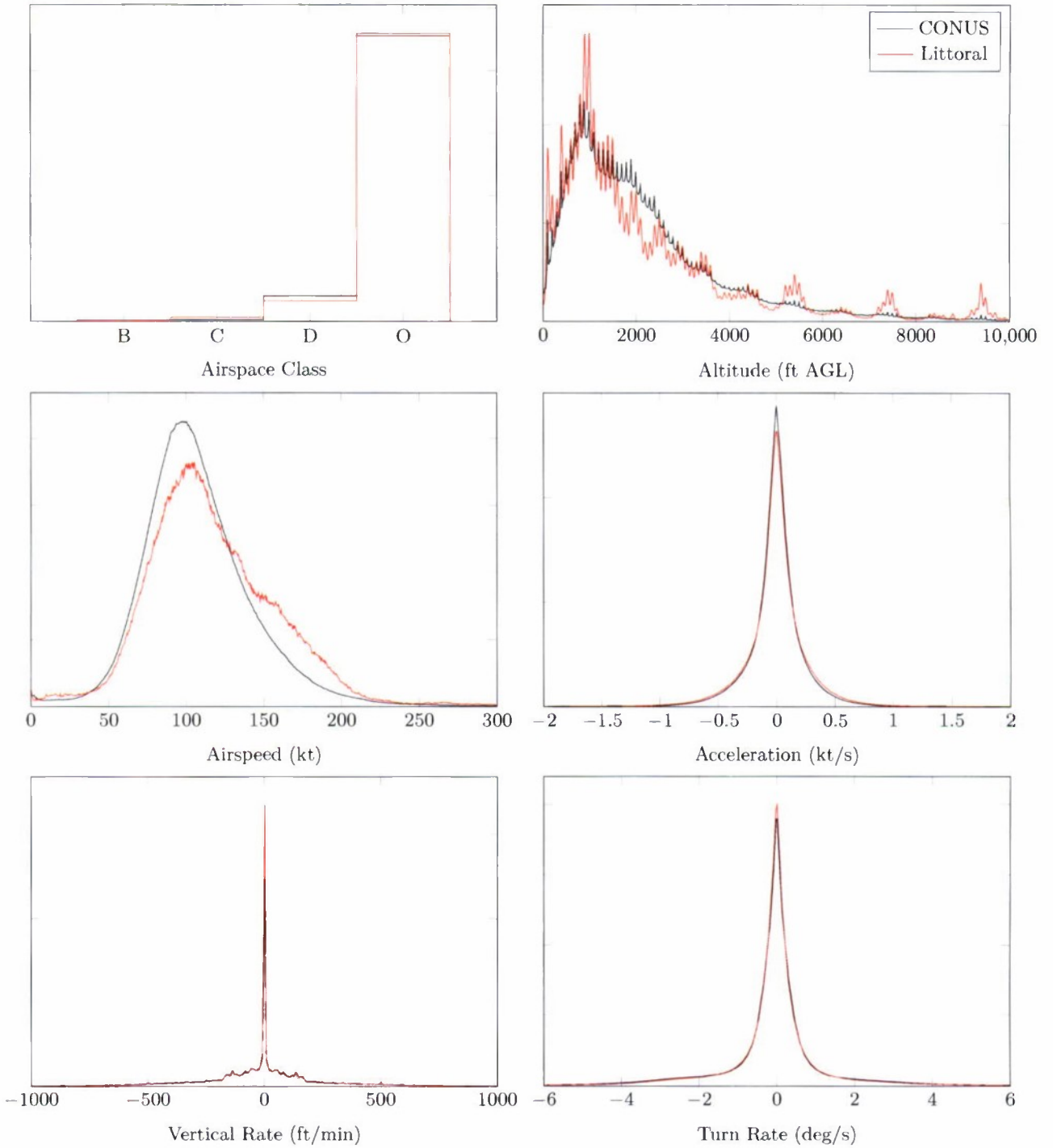
Figure A-2. Uncorrelated relative frequency feature comparison for continuous variables. Of note are the low period altitude oscillations which are caused by altitude quantization while the longer period littoral altitude oscillations correspond with standard VFR cruising altitudes—these are not present in the CONUS data due to terrain variation.
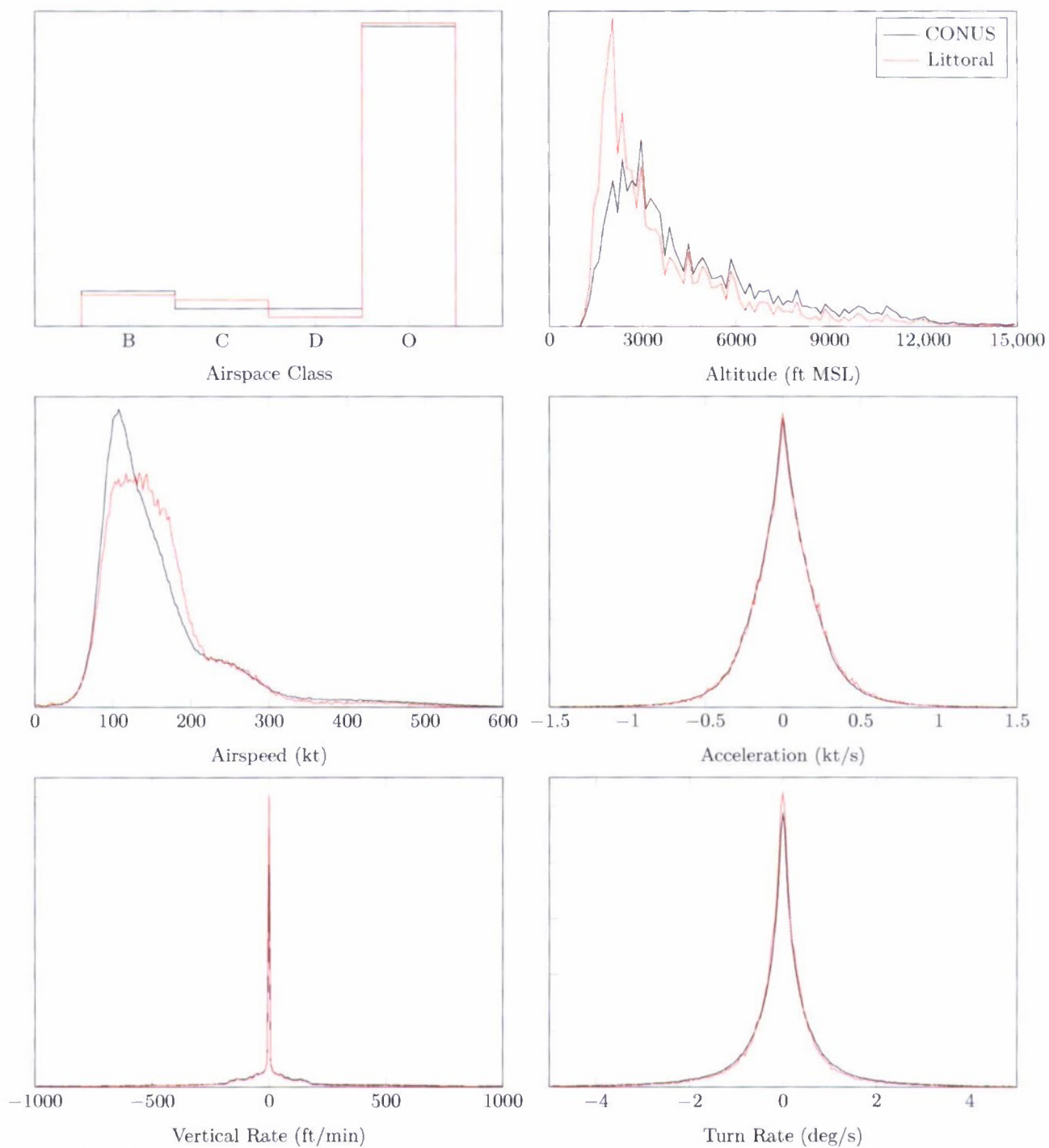
A.2 CORRELATED MODEL

Figure A-3. Correlated relative frequency feature comparison for continuous variables. The MSL altitude is the altitude of the higher aircraft at CPA.
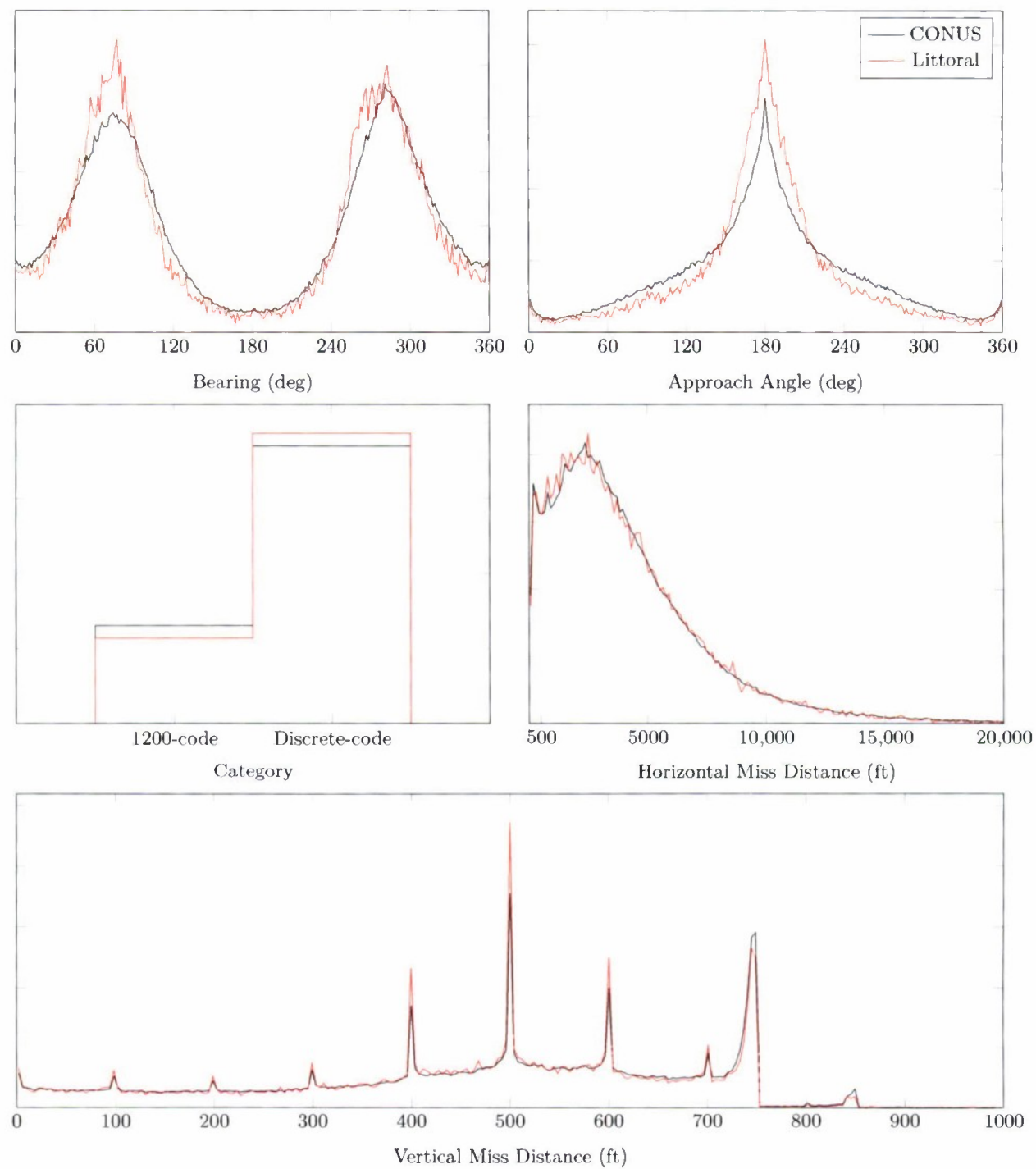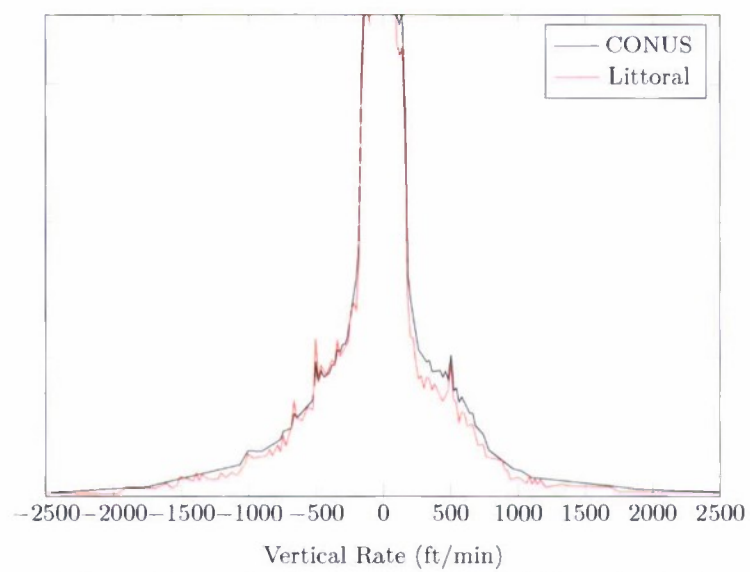
33

Figure A-4. Correlated relative frequency feature comparison for continuous variables defined at the closest point of approach.

Figure A-5. Aircraft vertical rate in correlated encounters magnified for detailed view of distribution tails.

This page intentionally left blank.

APPENDIX B
MODEL VARIABLES

The model variables are reprinted from the CONUS model documentation for reference.

B.1 UNCORRELATED MODEL

There are six variables in the uncorrelated encounter model:

- **Airspace class** A**:** The airspace class variable was incorporated into the model to account for the variation in how aircraft fly in different airspace classes. This variable may take on one of four values: B, C, D, and O, indicating which class of airspace the aircraft is in. The values B, C, and D correspond to the controlled airspace classes defined by the FAA. The value O represents "other airspace," including airspace Classes E and G. Note that there should be no VFR aircraft in Class A due to the requirement that aircraft in that Class of airspace fly under Instrument Flight Rules.

- **Altitude layer** L**:** Airspace is divided into four altitude layers, in a process similar to prior encounter models developed by Eurocontrol. The first layer spans from 500 to 1200 ft Above Ground Level (AGL) to capture aircraft in the traffic pattern or performing low-level maneuvers. The second layer spans a transition zone from 1200 to 3000 ft AGL, the cruise altitude where the hemispheric rule begins. The third layer spans from 3000 ft AGL to 5000 ft AGL covering a mix of low-altitude enroute and maneuvering aircraft. The fourth layer includes airspace above 5000 ft AGL and would cover most enroute VFR traffic.

- **Airspeed** v**:** We model true airspeed and allow it to vary during flight.

- **Acceleration** $\dot{v}$**:** We allow airspeed acceleration to vary every second, providing higher-fidelity motion than prior models.

- **Turn rate** $\dot{\psi}$**:** Turn rate is permitted to change every second in our model. The prior European and ICAO cooperative models allowed only a single turn during an encounter.

- **Vertical rate** $\dot{h}$**:** The vertical rate is permitted to change at every second. All prior cooperative models allowed only a single vertical acceleration period during an encounter.

B.2 CORRELATED MODEL

The aircraft at the higher altitude at TCA is called AC1. The other aircraft is called AC2. The remainder of this section explains how we model the relationship between the behavior of these two aircraft. We model the following variables to describe each encounter:

- **Vertical Miss Distance** *vmd*: Vertical miss distance is defined as the difference in altitude between the two aircraft at the point of closest approach (point of minimum horizontal miss distance).

- **Horizontal Miss Distance** *hmd*: Horizontal miss distance is defined as the horizontal range between the two aircraft at the point of closest approach (point of minimum horizontal miss distance).

- **Airspace class** A: This variable may take on one of four values: B, C, D, and O, indicating which class of airspace the encounter is in. The values B, C, and D correspond to the controlled airspace classes defined by the FAA. The value O represents "other airspace," which includes Class A, E, and G airspace. The airspace class variable was incorporated into the model to account for the variation in how aircraft fly in different airspace classes. Note that Class A can be distinguished from Classes E and G by referring to the next variable: altitude layer.

- **Altitude layer** L: Airspace is divided into five altitude layers, similar to prior encounter models developed by Eurocontrol. The first layer spans from 1000 to 3000 ft Above Ground Level (AGL) to capture encounters in the traffic pattern. Encounters that occur below 1000 ft AGL are filtered out; TCAS, for example, will not issue resolution advisories for encounters occurring below 1000 ft AGL. The second layer spans from 3000 ft AGL to 10,000 ft Mean Sea Level (MSL), the upper limit for aircraft without transponders and the 250 kt airspeed restriction. The third layer spans from 10,000 ft MSL to FL180, the upper limit for VFR traffic and the beginning of Class A airspace. The fourth layer spans from FL180 to FL290, the beginning of the Reduced Vertical Separation Minimum (RVSM). The fifth layer includes all airspace above FL290. The altitude layer for an encounter is determined by the altitude of AC1 at TCA.

- **Approach Angle** β: Approach angle is the heading of AC2 relative to AC1 at TCA. Figure B-1 shows how β is calculated. The European encounter models also used this definition.

- **Bearing** χ: Figure B-1 shows how the bearing of AC2 relative to AC1 is calculated at TCA. Given β, *hmd*, and χ, we can uniquely identify the lateral position and orientation of AC2 relative to AC1 at TCA.

- **Category** C_1 **and** C_2: We currently divide aircraft into two categories: 1200-code aircraft and discrete-code aircraft. Compared to discrete-code aircraft, aircraft squawking 1200 tend to accelerate more frequently, fly at lower altitudes and at lower speeds, and are often smaller aircraft.

- **Initial Airspeed** v_1 **and** v_2: We model initial airspeeds of the two aircraft. We assume zero wind since aircraft close enough to be in an encounter situation are most likely within the same air mass and experiencing approximately the same windfield.

- **Acceleration** $\dot{v}_1$ **and** $\dot{v}_2$: The model assumes constant airspeed acceleration for the duration of the encounter as was the case in the prior European encounter models. This is a reasonable approximation given the short 50 s duration of each encounter.

- **Turn rate** $\dot{\psi}_1$ **and** $\dot{\psi}_2$: Turn rate is permitted to change every second in the model. The prior European and ICAO models allowed only a single turn during an encounter.

- **Vertical rate** $\dot{h}_1$ **and** $\dot{h}_2$: The vertical rate is permitted to change at every second. All prior cooperative models allowed only a single vertical acceleration period during an encounter.
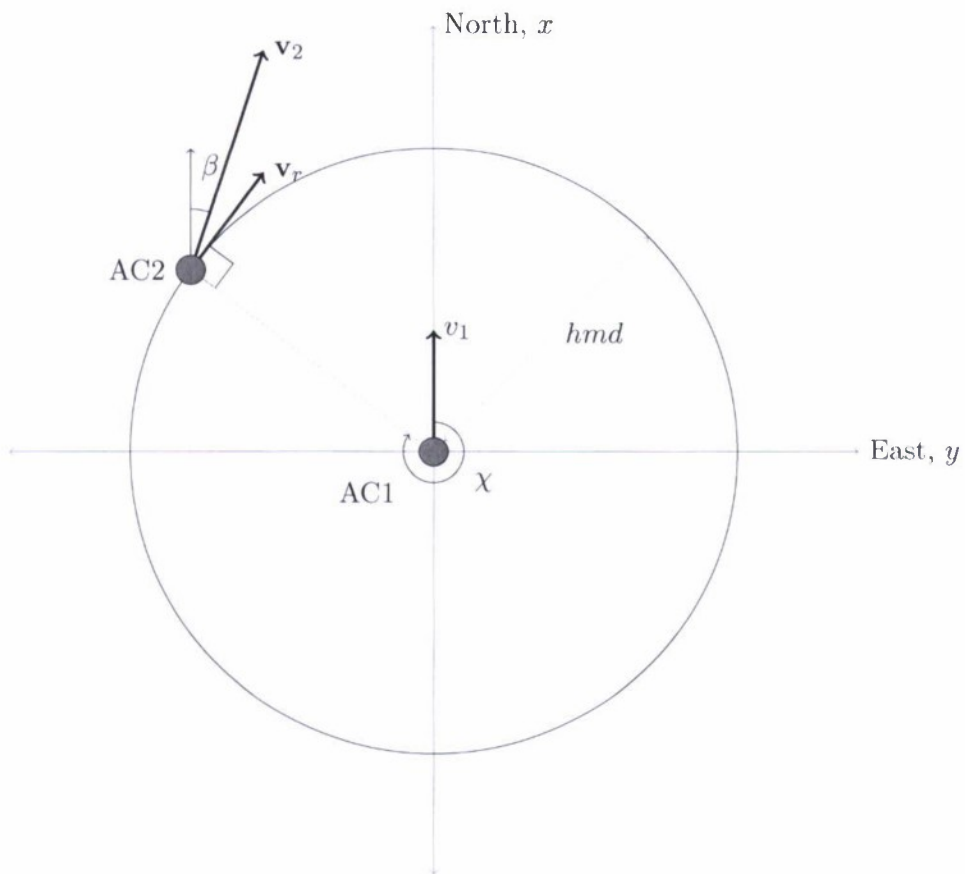
Figure B-1. Approach angle (β) and bearing (χ) definition.

This page intentionally left blank.

APPENDIX C
UNCORRELATED MODEL ADDENDUM

Section 6.1 of the uncorrelated model documentation described the process for estimating the NMAC probability [7]. The method for estimating the NMAC probability in this section should be used in its place. The process for initializing uncorrelated encounters is reprinted here for reference followed a description of the modifications to the NMAC probability calculation.

C.1 ENCOUNTER INITIALIZATION

We use rejection sampling to generate the initial conditions of an encounter. Rejection sampling involves proposing a series of candidate samples from a random distribution until choosing one that meets a set of criteria. The process we use for generating initial conditions for encounters is as follows:

1. Generate airspeeds, vertical rates, turn rates, and accelerations for AC1 and AC2 according to their models such that they belong to the same airspace class and altitude layer. Forcing this constraint can be done using rejection sampling. Simply generate AC1 and AC2 independently and reject both if they have a different airspace class or altitude layer.[1] AC1 and AC2 are termed the own and intruder aircraft, respectively.

2. Initialize the position of AC2 on the surface of the encounter cylinder centered on AC1. AC2 may be initialized on the top, bottom, or side surfaces of the encounter cylinder. The probability of being located on the top, bottom, or side is proportional to the volume swept out by each encounter cylinder surface. Once top, bottom, or side has been selected, AC2 is randomly positioned using a two-dimensional uniform distribution across that surface. The bearing of AC2 relative to AC1 is denoted χ.

3. The heading of AC1 is set to zero for simplicity. The heading of AC2, denoted ψ, is randomly selected from a uniform distribution over $[\pi, \pi)$.

4. If AC2 was initialized on the top of the encounter cylinder, accept the sample if the vertical rate of AC2 relative to AC1, denoted $v_{R,v}$, is negative. This ensures that AC2 is penetrating the encounter cylinder for the first time.

5. If AC2 was initialized on the bottom of the encounter cylinder, accept the sample if the vertical rate of AC2 relative to AC1, denoted $v_{R,v}$, is positive. This ensures that AC2 is penetrating the encounter cylinder for the first time.

6. If AC2 was initialized on the side of the encounter cylinder, accept the sample if $\hat{\mathbf{R}} \cdot \mathbf{v}_{R,h}$ is negative, where $\hat{\mathbf{R}} = (\sin \chi, \cos \chi)$ is the representation of the horizontal unit vector from AC1 to AC2 in the (East, North) coordinate frame and $\mathbf{v}_{R,h}$ is $\mathbf{v}_2 - \mathbf{v}_1$. The vectors $\mathbf{v}_1$ and $\mathbf{v}_2$

---

[1]Note that this will result in an incorrect distribution over airspace class and layer (compared to that observed). Reference Section C.4 for the proper correction.

are the horizontal ground velocities of AC1 and AC2 respectively. When $\hat{\mathbf{R}} \cdot \mathbf{v}_{R,h}$ is negative, the relative velocity of AC2 with respect to AC1 is into the encounter cylinder, and therefore the encounter should be accepted.

The process is repeated until a candidate initialization is accepted. A byproduct of rejection sampling is that the intruder bearing distribution is nonuniform. As one would expect, more encounters occur head on than from the side or rear. Figure C-1 illustrates the initial horizontal variables for uncorrelated encounters at the instant when the intruder aircraft penetrates the side of the encounter cylinder.
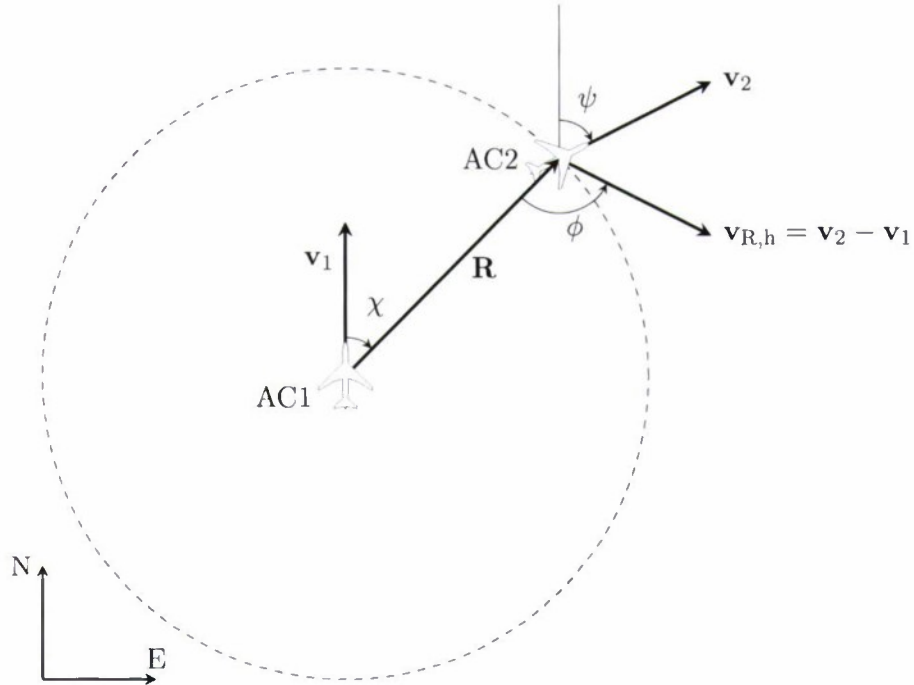

Figure C-1. Horizontal plane encounter initialization.

C.2   ESTIMATING NMAC PROBABILITY

This initialization procedure is the result of the fundamental assumption that the two aircraft blunder into close proximity. The penetration angle (ϕ) represents the scalar projection of the relative horizontal velocity ($\mathbf{v}_{R,h}$) onto the radial vector ($\mathbf{R}$) and is a function of the initial intruder bearing, intruder heading, and the initial horizontal airspeeds of the aircraft. An encounter is defined only if the intruder penetrates the encounter cylinder—ϕ must be on the interval $(-\pi/2, \pi/2)$. Therefore, the encounter depicted by Figure C-1 would be rejected and a new encounter would need to be initialized. A similar procedure is required for intruders that penetrate the top or bottom of the encounter cylinder.

Ideally, the encounter parameters would be sampled according to the appropriate probability distributions describing the expected encounter geometry. If encounters were sampled according to the appropriate distributions, then the NMAC probability estimate would simply be the number of encounters resulting in NMACs normalized by the total number of simulated encounters. There are three a posteriori corrections that must be used when estimating the NMAC probability.

1. Encounters are more likely to occur among aircraft with higher relative airspeeds, but airspeeds are sampled from the distribution of observed aircraft airspeeds.

2. When the intruder penetrates the side face of the cylinder, the initial bearing and heading of the intruder are sampled uniformly, but intruder bearings and headings which result in a penetration angle nearer to zero are more likely. In other terms, encounters where the relative velocity penetrates the encounter cylinder directly are more likely to occur than when the relative velocity skims the edge of the encounter cylinder.[2]

3. Encounters are not generated with the correct proportion of intruders penetrating the top or bottom of the cylinder compared to the side of the cylinder. The true proportion is derived from the volume that each face of the encounter cylinder sweeps out per unit time. Hence, the effort of estimating $P(\text{nmac} \mid \text{enc})$ may be decoupled into the horizontal and vertical components and then combined into an overall estimate.

Since encounters are not sampled from the actual distributions, the encounters must be weighted to compensate for the difference between the actual and sampling distributions. This process is known as importance sampling [23]. The general process for estimating $P(\text{nmac} \mid \text{enc})$ using the actual distribution $p(x)$ and the sampling distribution $q(x)$ is

$$P(\text{nmac} \mid \text{enc}) = \frac{\sum_i f(x^{(i)}) \frac{p(x^{(i)})}{q(x^{(i)})}}{\sum_i \frac{p(x^{(i)})}{q(x^{(i)})}} , \tag{C-1}$$

where $f(x)$ is the probability of an NMAC given the generated samples $(x^{(i)})$, where i denotes an encounter sample. It should be noted that $f(x)$ is not constrained to be $P(\text{nmac} \mid \text{enc})$, but rather any metric—e.g., vertical miss distance, course deviation. Because the summation of the weights is generally unnormalized (does not sum to unity), we must normalize by the term $\sum_i p(x^{(i)})/q(x^{(i)})$.

The weighting to correct the improper sampling of airspeeds and the penetration angle is described by

$$\frac{p(x^{(i)})}{q(x^{(i)})} = \begin{cases} v_{R,h}^{(i)} \cos \phi^{(i)} & \text{for initialization on side of cylinder} \\ v_{R,v}^{(i)} & \text{for initialization on top/bottom of cylinder} \end{cases} . \tag{C-2}$$

The term $\cos \phi$ is equivalent to $-\hat{\mathbf{v}}_{R,h} \cdot \hat{\mathbf{r}}$. The average relative volume that the encounter cylinder sweeps out per unit time is

$$\bar{V} = 4 r_{\text{enc}} h_{\text{enc}} \bar{v}_{R,h} + \pi r_{\text{enc}}^2 \bar{v}_{R,v} , \tag{C-3}$$

---

[2]Section C.3 describes the method for accounting for this correction when initializing encounters.

where $\bar{v}_{\mathrm{R,h}}$ and $\bar{v}_{\mathrm{R,v}}$ are the magnitudes of the average relative horizontal and vertical airspeeds between any two aircraft in the airspace, respectively. Note that $\bar{v}_{\mathrm{R,h}}$ and $\bar{v}_{\mathrm{R,v}}$ are not the relative airspeeds between pairs of aircraft that result in an encounter, but rather between any two aircraft in the airspace. Therefore, they do not need to be weighted to adjust for those pairs resulting in encounters. The average relative airspeeds may be estimated directly from the sample mean of the initial relative airspeed—e.g., $\bar{v}_{\mathrm{R,h}} = 1/N \sum_i v_{\mathrm{R,h}}^{(i)}$. The encounter rate is

$$\lambda_{\mathrm{enc}} = \rho \bar{V} \,, \tag{C-4}$$

where ρ is the airspace density [31]. The NMAC rate is therefore defined by

$$\lambda_{\mathrm{nmac}} = P(\mathrm{nmac} \mid \mathrm{enc}) \lambda_{\mathrm{enc}} \,. \tag{C-5}$$

It should be noted that this formation of the encounter rate (Equation C-4) is the rate at which a single aircraft encounters a population of intruder aircraft as opposed to the rate of all encounters between any two aircraft in a specified airspace.

From Equation C-3, the total volume swept out by the encounter cylinder can be decoupled into horizontal and vertical components. The ratio of the number of encounters penetrating the side of the encounter cylinder (n_{h}) to the number penetrating the top or bottom (n_{v}) is proportional to the ratio of the horizontal and vertical swept volumes, or

$$\frac{n_{\mathrm{h}}}{n_{\mathrm{v}}} = \frac{\bar{V}_{\mathrm{h}}}{\bar{V}_{\mathrm{v}}} = \frac{4 r_{\mathrm{enc}} h_{\mathrm{enc}} \bar{v}_{\mathrm{R,h}}}{\pi r_{\mathrm{enc}}^2 \bar{v}_{\mathrm{R,v}}} \,. \tag{C-6}$$

Expanding Equation C-1 with the weighting of Equation C-2 and correcting for the proportion of encounters penetrating each cylinder surface results in the NMAC probability formulation

$$P(\mathrm{nmac} \mid \mathrm{enc}) = \left(\frac{\sum_i v_{\mathrm{R,h}}^{(i)} \cos \phi^{(i)} f(x^{(i)})}{\sum_i v_{\mathrm{R,h}}^{(i)} \cos \phi^{(i)}} \right) \frac{4 r_{\mathrm{enc}} h_{\mathrm{enc}} \bar{v}_{\mathrm{R,h}}}{\bar{V}} + \left(\frac{\sum_j v_{\mathrm{R,v}}^{(j)} f(x^{(j)})}{\sum_j v_{\mathrm{R,v}}^{(j)}} \right) \frac{\pi r_{\mathrm{enc}}^2 \bar{v}_{\mathrm{R,v}}}{\bar{V}} \,. \tag{C-7}$$

Indices i and j denote encounter samples where the intruder penetrates the horizontal and vertical surfaces of the cylinder, respectively. The terms in parenthesis correct for the improper sampling of the relative airspeed and the penetration angle, while the term outside of the parenthesis corrects for the improper proportion of intruders initialized on each cylinder surface.

C.3   ALTERNATIVE SAMPLING METHODOLOGY

The method described above for initializing AC2 on the side of the encounter cylinder centered on AC1 is intuitive. But, this method results in an abundance of short encounters where the closest point of approach (defined at the minimum horizontal separation) is near the radius of the encounter cylinder. These short encounters, on the order of 10 s, do not affect the NMAC probability because an avoidance maneuver is very unlikely. In addition, the standard method for initializing encounters also does not allow for the explicit definition of the CPA distribution, which is useful when the analyst wants to focus computation on close encounter situations (i.e., NMACs). The procedure
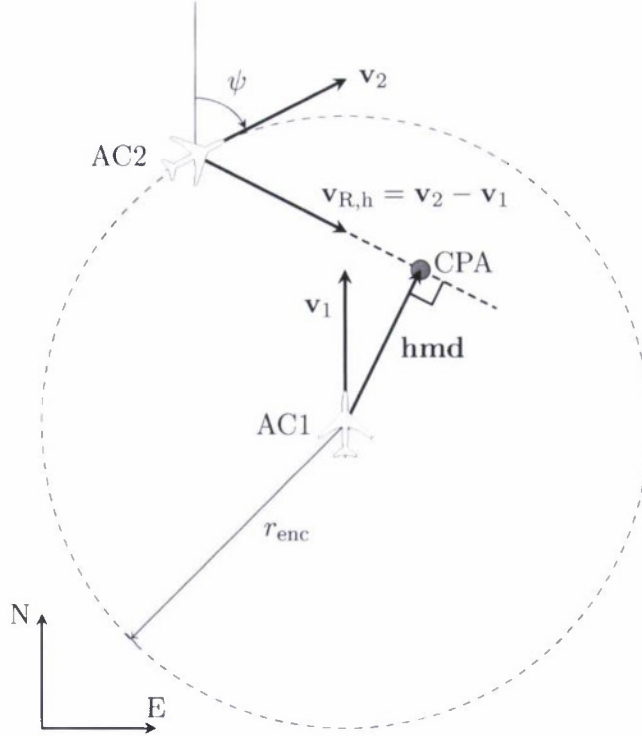
Figure C-2. Alternative horizontal plane sampling methodology illustration.

as described below is illustrated in Figure C-2 and replaces step (2) in Section C.1 for horizontal encounters. Step (6), which ensures that the intruder penetrates the encounter cylinder, is no longer necessary.

1. Instead of initializing intruder aircraft on the horizontal face of the encounter cylinder by uniformly sampling the initial relative bearing (χ), intruder aircraft are initialized by uniformly sampling the horizontal miss distance (HMD) on the interval $[0, r_{\text{enc}})$.

2. The intruder aircraft (AC2) is notionally placed a distance HMD from AC1 at CPA. AC2 may be placed in front or behind AC1. Each is equally probable, so one should sample uniformly over the two options.

3. The CPA, assuming straight line trajectories, is the position where the sampled HMD is satisfied together with the condition that **hmd** is perpendicular to $\mathbf{v}_{R,h}$. The vector **hmd** is the position vector from AC1 to the CPA.

4. AC2 is then placed on the encounter cylinder by finding the intersection of $\mathbf{v}_{R,h}$ with the horizontal cylinder boundary. This procedure is accomplished such that the intruder penetrates the encounter cylinder at initialization.

The sampling of the intruder aircraft heading is left unchanged. The initial relative altitude, defined at penetration of the encounter cylinder, is sampled uniformly on the interval $[-h_{\text{enc}}, h_{\text{enc}}]$. Note

that the notional CPA created during this process is unlikely to be realized during simulation because $\mathbf{v}_{\mathrm{R,h}}$ is the initial relative airspeed and is therefore likely to change during the encounter—i.e., it is only used for this initialization procedure. When using this encounter initialization method, the term $\cos\phi$ is no longer needed in Equation C-7, resulting in

$$P(\mathrm{nmac} \mid \mathrm{enc}) = \left(\frac{\sum_i v_{\mathrm{R,h}}^{(i)} f(x^{(i)})}{\sum_i v_{\mathrm{R,h}}^{(i)}}\right) \frac{4 r_{\mathrm{enc}} h_{\mathrm{enc}} \bar{v}_{\mathrm{R,h}}}{\bar{V}} + \left(\frac{\sum_j v_{\mathrm{R,v}}^{(j)} f(x^{(j)})}{\sum_j v_{\mathrm{R,v}}^{(j)}}\right) \frac{\pi r_{\mathrm{enc}}^2 \bar{v}_{\mathrm{R,v}}}{\bar{V}} . \qquad (C\text{-}8)$$

Note that this procedure is only for encounters initialized on the side face of the encounter cylinder. Although it is beyond the scope of this document, a similar procedure may be used to initialize encounters when the encounter volume is a sphere. If enough aircraft tracks (encounter model samples) are formed prior to encounter initialization, a high-confidence estimate of the ratio of intruders penetrating each face could be formed according to Equation C-6. This estimate could then be used to correctly sample the encounter cylinder penetration face, removing the need for each cylinder face contribution to the swept volume in Equation C-8.

C.4 ALTITUDE LAYER AND CLASS WEIGHTING

Encounters are generated according to the altitude layer and airspace class distributions defined in the model. These distributions represent the observed rate of occurrence of aircraft in each altitude layer and airspace class. But from Equation C-4, the encounter rate is proportional to the airspace density, not the cumulative occurrence of aircraft, in the local airspace. For example, the greatest observed cumulative occurrence (total flight time) of aircraft is found in the airspace defined as "other" in the model (corresponding to class E and G airspace), but this airspace also occupies the largest volume. Furthermore, the model assumes that the exposure time (t_e), or the duration of time that the own aircraft operates in each airspace, is equally divided amongst each airspace class and layer. Therefore, the mean NMAC probability over all airspace classes and altitude layers that considers these factors a posteriori is defined by

$$\bar{P}(\mathrm{nmac} \mid \mathrm{enc}) = \sum_i P(\mathrm{nmac} \mid \mathrm{enc}, a_i, l_i) P(a_i, l_i \mid \mathrm{enc}) = \frac{\sum_i P(\mathrm{nmac} \mid \mathrm{enc}, a_i, l_i) \rho_i \bar{V}_i t_e^{(i)}}{\sum_i \rho_i \bar{V}_i t_e^{(i)}} , \quad (C\text{-}9)$$

where i denotes each airspace class and altitude layer combination. The term $P(a_i, l_i \mid \mathrm{enc})$ is the proportion of encounters expected in each altitude layer and airspace class combination.

If one knows ρ_i, $\bar{V}_i$, and $t_e^{(i)}$ a priori, then the altitude and airspace class distributions can be modified to reflect this knowledge before sampling from the model. Then, the mean NMAC probability estimate is simply the NMAC probability for all encounters. This sampling procedure may be useful when the aircraft of interest is expected to operate in a specific airspace class or altitude layer. For example, some aircraft types may only operate in the first altitude band (500–1200 ft AGL), thus simulating encounters in the other layers wastes computation because they will not be considered in the final estimate. If little is known about the expected operating environment, then an objective (uniform) assumption regarding the airspace class and altitude layer may be suitable.

APPENDIX D
NETWORK STRUCTURE CANDIDATES

This section describes the network candidates that were considered for the littoral models. The optimal network was chosen by maximizing the Bayesian network score (Equation E-7). The optimal scores are denoted and the optimal CONUS models are shown for reference. The same set of networks that was considered for the CONUS models was considered for the littoral models. The candidate model structures were selected based on expert knowledge, previous encounter model structures, and automated search techniques.

D.1   UNCORRELATED CANDIDATES

D.1.1   Initial Network Candidates
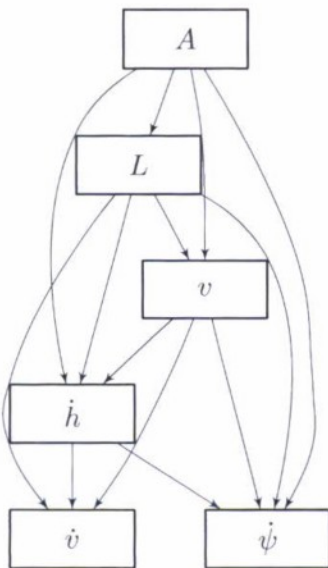
(1) Edges: 13, Parameters: 7167

Model	Score
Littoral	-38156685
CONUS	-967535636
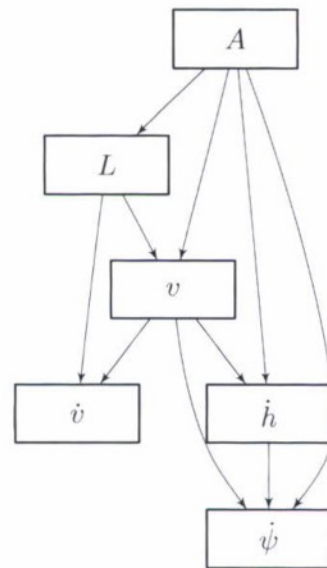
(2) Edges: 10, Parameters: 1791

Model	Score
Littoral	-38596563
CONUS	-975857519
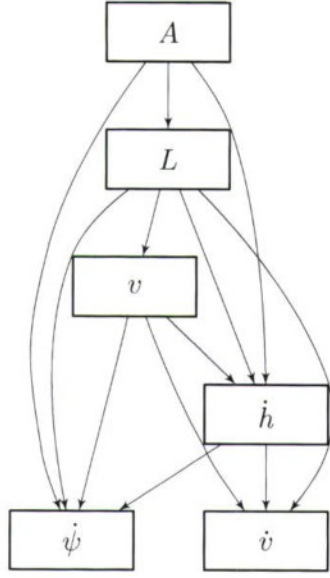
(3) Edges: 12, Parameters: 7083

Model	Score
Littoral	-38187483
CONUS	-968008451
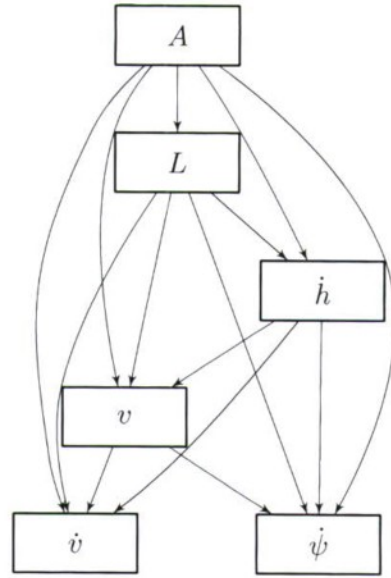
(4) Edges: 14, Parameters: 9855

Model	Score
Littoral	-38090950
CONUS	-966680903
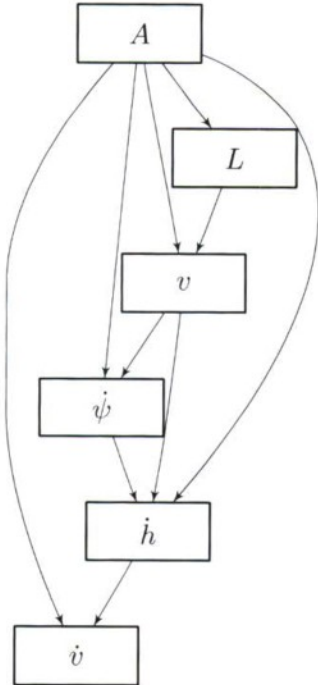
(5) Edges: 10, Parameters: 1775

Model	Score
Littoral	-38475107
CONUS	-974521777
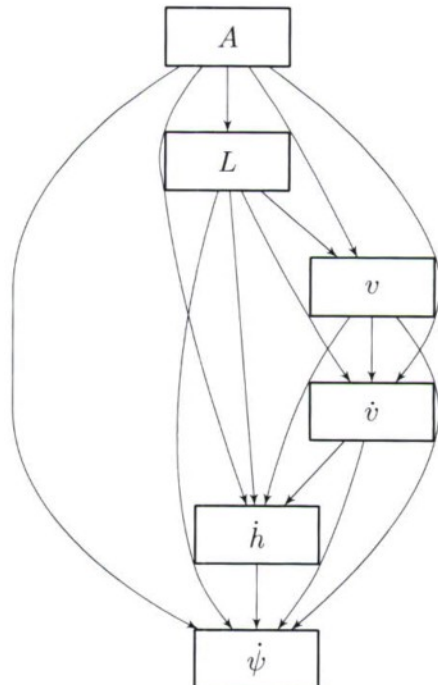
(6) Edges: 15, Parameters: 31,359

Model	Score
Littoral (Best)	-37927856
CONUS (Best)	-961629997
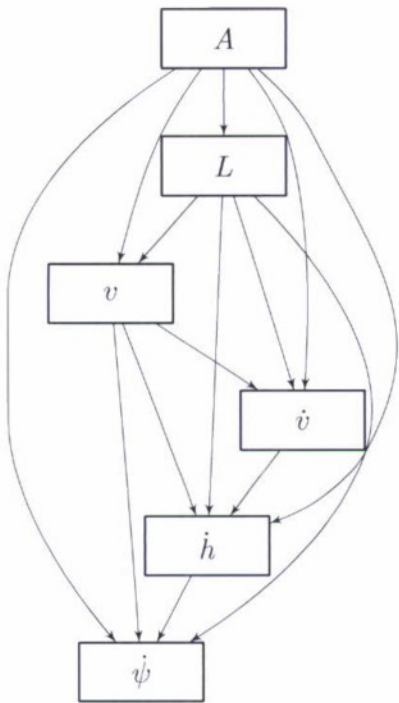
(7) Edges: 14, Parameters: 9855

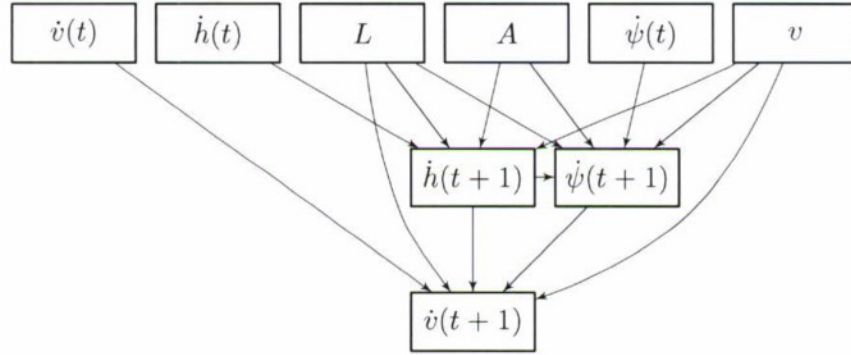| Model	Score
Littoral	-38091977
CONUS	-966681414
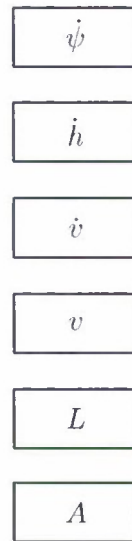
(8) Edges: 0, Parameters: 29

Model	Score
Littoral	-39924524
CONUS	-1013111341

D.1.2 Transition Network Candidates
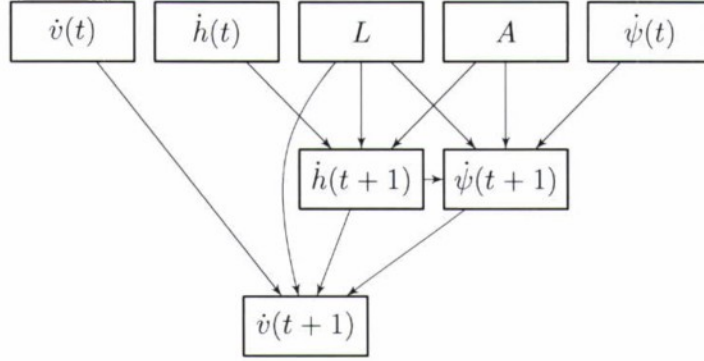
(1) Edges: 11, Parameters: 9296

Model	Score
Littoral	-1113146
CONUS	-29392892

(2) Edges: 14, Parameters: 74,368

Model	Score
Littoral	-1173002
CONUS	-29213939

$\dot{v}(t)$ $\quad$ $\dot{h}(t)$ $\quad$ A $\quad$ L $\quad$ $\dot{\psi}(t)$ $\quad$ v

$\dot{h}(t+1)$ $\quad$ $\dot{\psi}(t+1)$

$\dot{v}(t+1)$
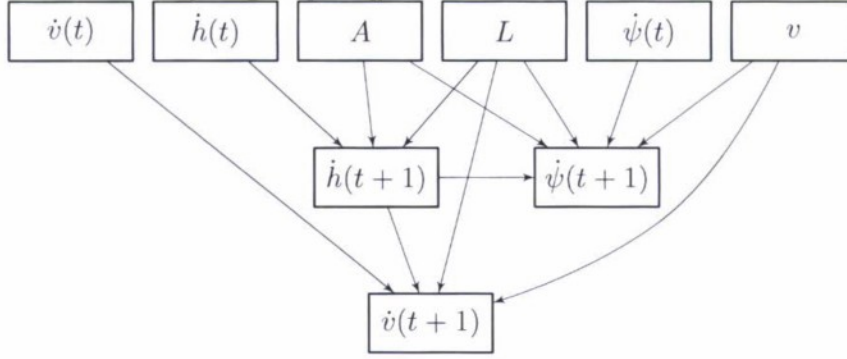
(3) Edges: 12, Parameters: 42,784

Model	Score
Littoral	-1136239
CONUS	-29251530

$\dot{v}(t)$ $\quad$ $\dot{h}(t)$ $\quad$ A $\quad$ L $\quad$ v $\quad$ $\dot{\psi}(t)$

$\dot{h}(t+1)$ $\quad$ $\dot{\psi}(t+1)$

$\dot{v}(t+1)$
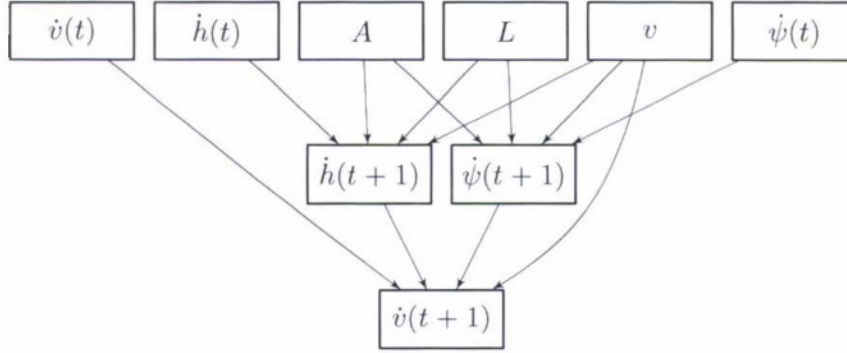
(4) Edges: 12, Parameters: 18,592

Model	Score
Littoral	-1122499
CONUS (Best)	-29173494
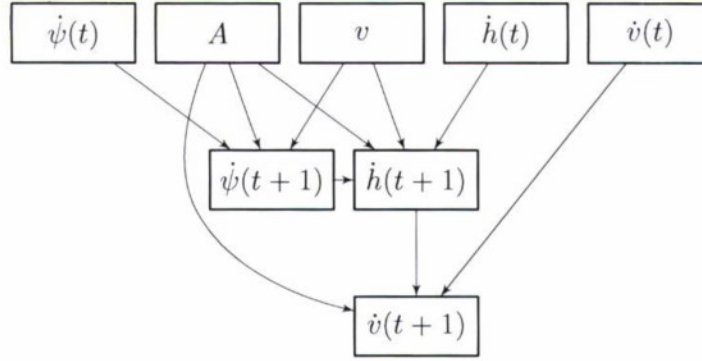
(5) Edges: 10, Parameters: 11,312

Model	Score
Littoral	-1110877
CONUS	-29391204
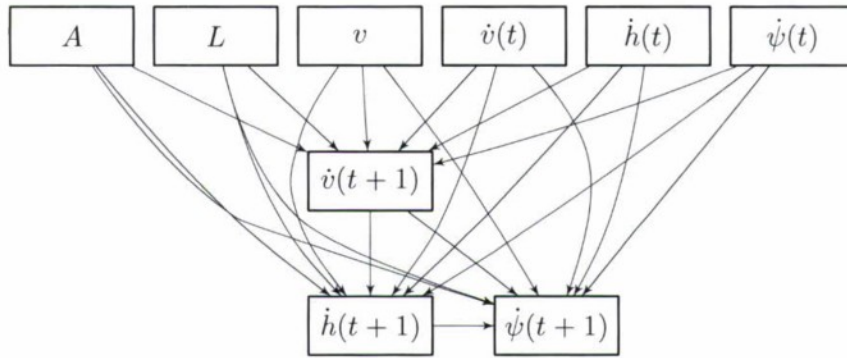
(6) Edges: 21, Parameters: 7,651,840

Model	Score
Littoral	-1370034
CONUS	-29790622
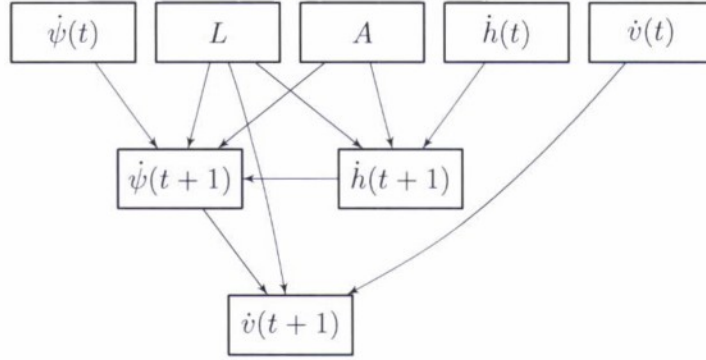
(7) Edges: 10, Parameters: 5936

Model	Score
Littoral (Best)	-1106490
CONUS	-29464867

(8) Edges: 0, Parameters: 16

Model	Score
Littoral	-15439646
CONUS	-407569877

D.2 CORRELATED CANDIDATES

D.2.1 Initial Network Candidates

A	L	χ	β	hmd	vmd

$\dot{\psi}_1$	$\dot{h}_1$	$\dot{v}_1$	v_1	C_1

$AC1$

$\dot{\psi}_2$	$\dot{h}_2$	$\dot{v}_2$	v_2	C_2

$AC2$
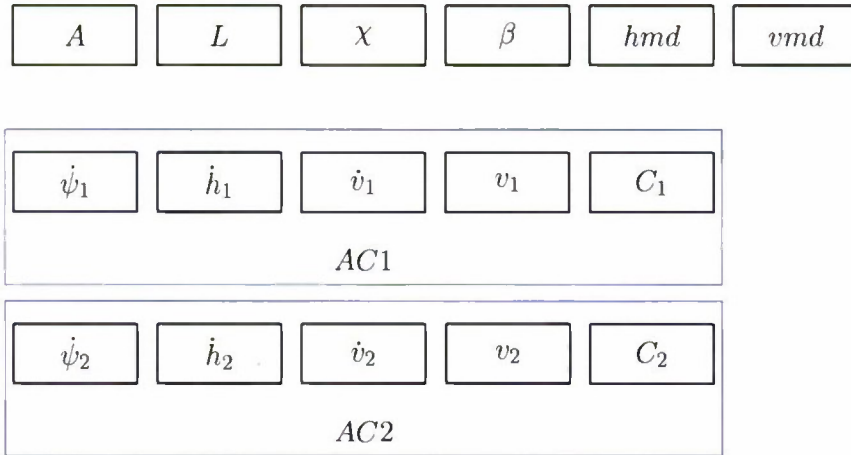
(1) Edges: 0, Parameters: 83

Model	Score
Littoral	-682309
CONUS	-7225886
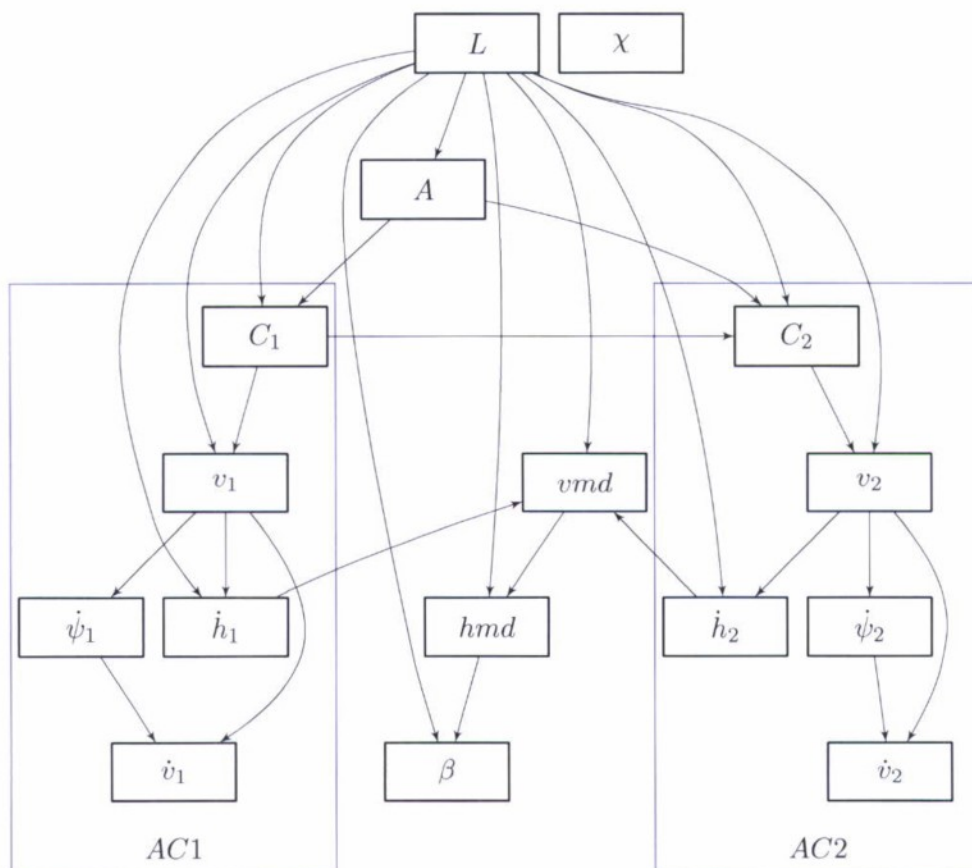
(2) Edges: 27, Parameters: 5203

Model	Score
Littoral	-646047
CONUS	-6746733
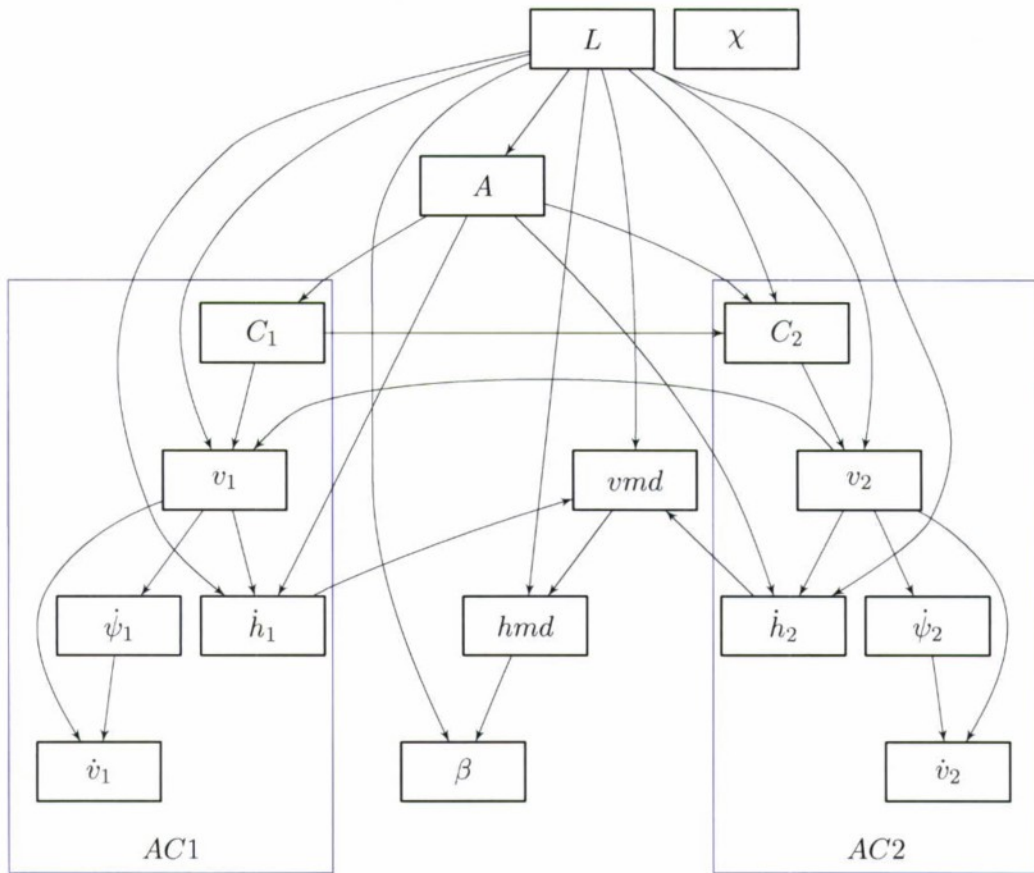
(3) Edges: 29, Parameters: 6877

Model	Score
Littoral	-645892
CONUS	-6743530
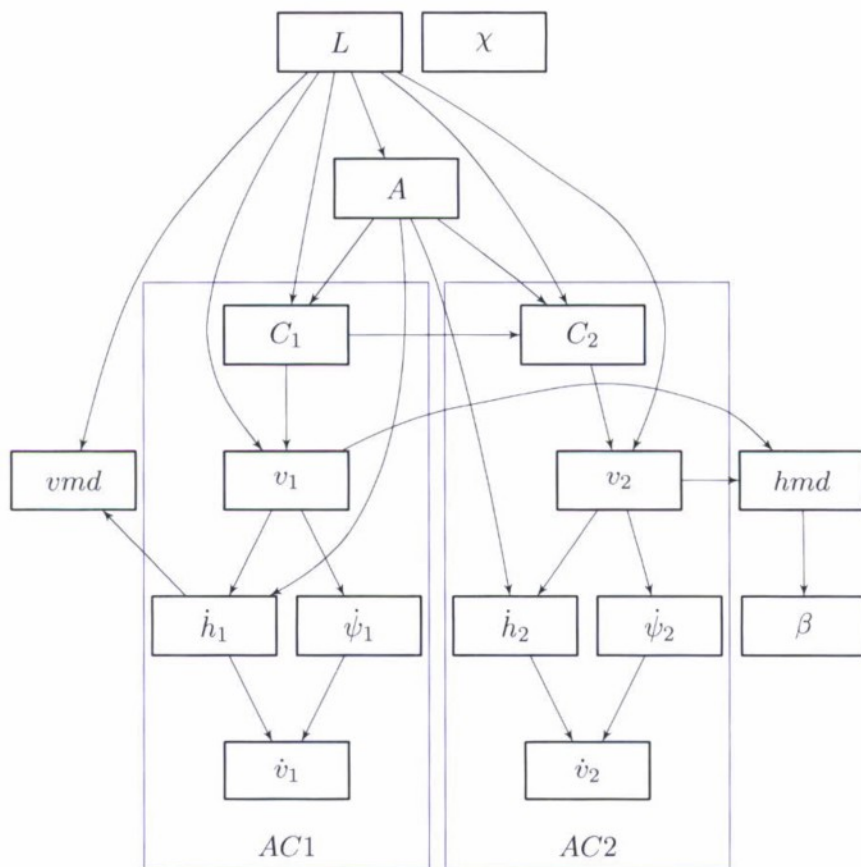
(4) Edges: 25, Parameters: 1865

Model	Score
Littoral	-648805
CONUS	-6783862
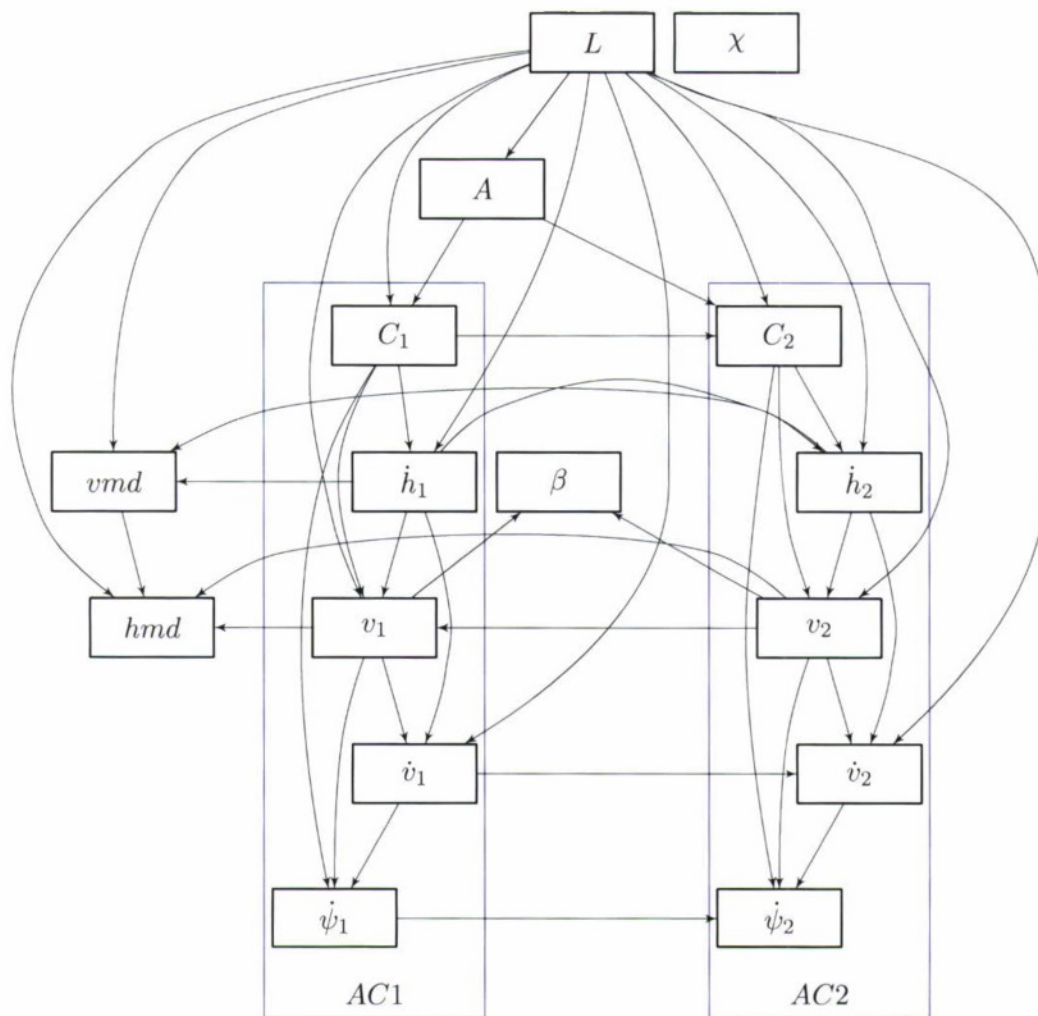
(5) Edges: 41, Parameters: 24,751

Model	Score
Littoral	-648264
CONUS	-6726995
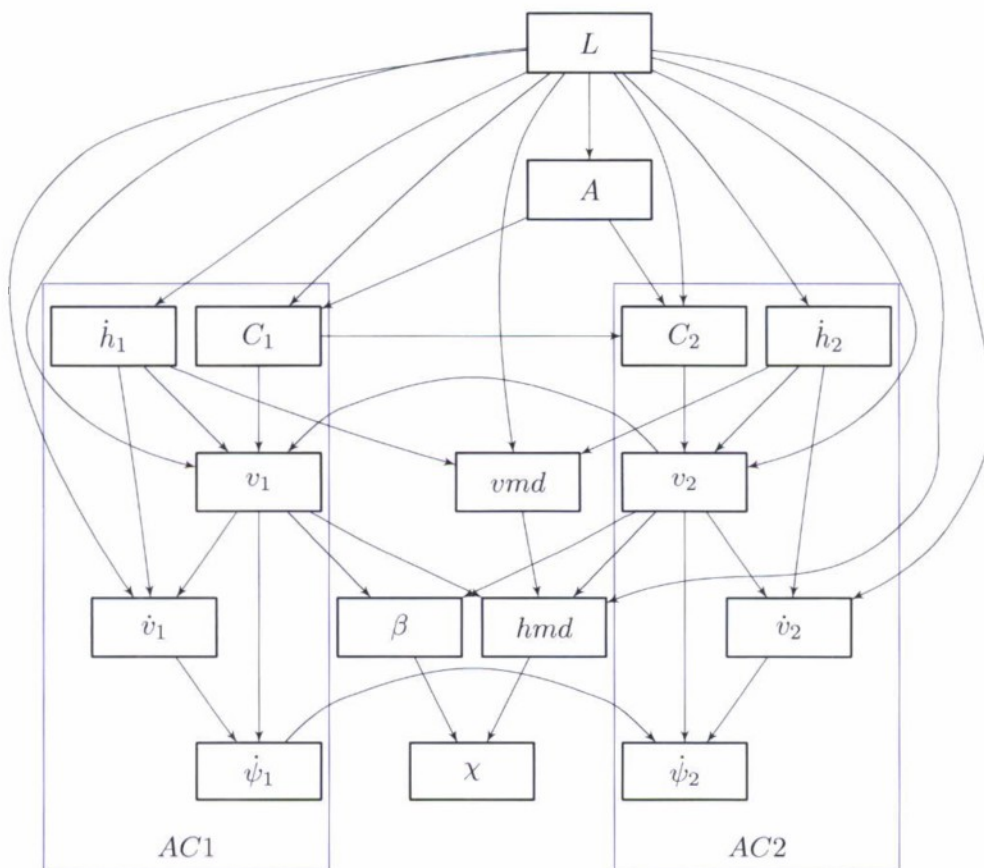
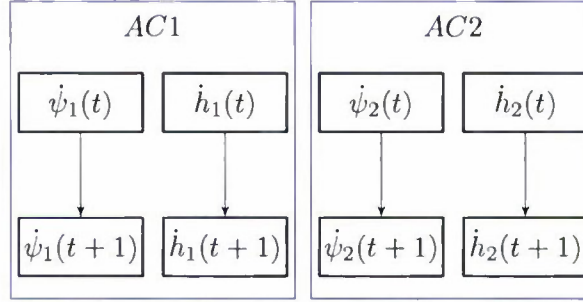(6) Edges: 37, Parameters: 17,358

Model	Score
Littoral	-643437 (Best)
CONUS	-6700437 (Best)

D.2.2 Transition Network Candidates
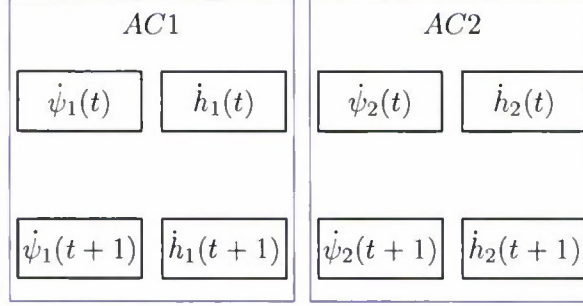
(1) Edges: 0, Parameters: 32

Model	Score
Littoral	-8396812
CONUS	-90986115

(2) Edges: 4, Parameters: 288

Model	Score
Littoral (Best)	-920981
CONUS	-9826752
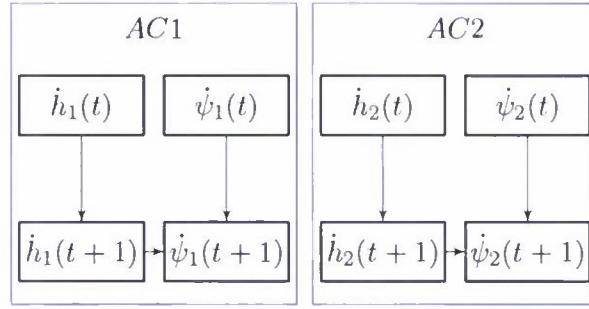
(3) Edges: 6, Parameters: 1440

Model	Score
Littoral	-925529
CONUS	-9828653
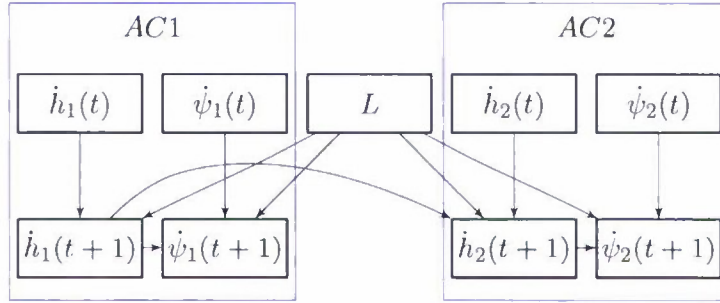
(4) Edges: 11, Parameters: 10,080

Model	Score
Littoral	-945592
CONUS	-9834130
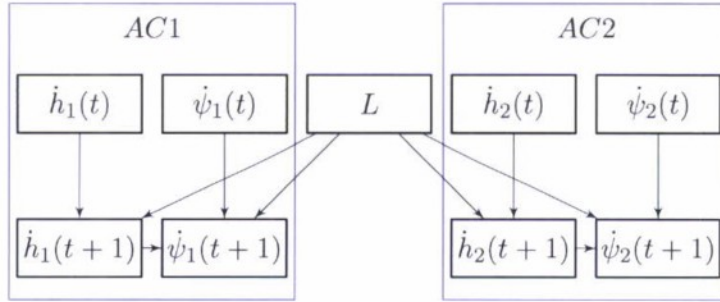
(5) Edges: 10, Parameters: 7200

Model	Score
Littoral	-938287
CONUS (Best)	-9822334

This page intentionally left blank.

APPENDIX E
BAYESIAN NETWORKS

This appendix briefly reviews Bayesian networks. Further discussion of Bayesian networks may be found elsewhere [32–34].

E.1 DEFINITION

A Bayesian network is a graphical representation of a multivariate probability distribution over variables $\mathbf{X} = X_1, \ldots, X_n$. In particular, a Bayesian network is a directed acyclic graph G whose nodes correspond to variables and edges correspond to probabilistic dependencies between them. Associated with each variable X_i is a conditional probability distribution $P(x_i \mid \pi_i)$, where π_i denotes an instantiation of the parents of X_i in the graph. The probability of an instantiation of the variables is specified directly by the conditional probability distributions in the Bayesian network:

$$P(\mathbf{x}) = P(x_1, \ldots, x_n) = \prod_{i=1}^{n} P(x_i \mid \pi_i). \tag{E-1}$$

E.2 SAMPLING

It is rather straightforward to sample from a multivariate distribution represented by a Bayesian network. The first step is to produce a topological sort of the nodes in the network. A topological sort orders the nodes in a Bayesian network such that if a node X_i comes before X_j there does not exist a directed path from X_j to X_i. Every Bayesian network has at least one topological sort, but there may be many. Efficient algorithms exist for finding a valid topological sort [35].

To produce a sample from the joint distribution represented by a Bayesian network, we simply iterate through a topologically sorted sequence of the variables and sample from their conditional probability distributions. The topological sort ensures that when sampling from each conditional probability distribution the necessary parents have been instantiated.

E.3 PARAMETER LEARNING

The parameters θ of a Bayesian network determine the associated conditional probability distributions. Given some fixed network structure G, we can learn these parameters from data. In this appendix, we assume that the variables are discrete.

Before discussing how to learn the parameters of a Bayesian network, it is necessary to introduce some notation. Let r_i represent the number of instantiations of X_i and q_i represent the number of instantiations of the parents of X_i. If X_i has no parents, then $q_i = 1$. The jth instantiation of the parents of X_i is denoted π_{ij}.

There are $\sum_{i=1}^{n} r_i q_i$ parameters in a Bayesian network. Each parameter is written θ_{ijk} and determines $P(X_i = k \mid \pi_{ij})$, i.e.,

$$P(X_i = k \mid \pi_{ij}) = \theta_{ijk} \,.$$

Although there are $\sum_{i=1}^{n} r_i q_i$ parameters, only $\sum_{i=1}^{n} (r_i - 1) q_i$ are independent.

Computing the posterior $p(\theta \mid D, G)$ involves specifying a prior $p(\theta \mid G)$ and applying Bayes' rule

$$p(\theta \mid D, G) = \frac{P(D \mid \theta, G) p(\theta \mid G)}{P(D \mid G)} = \frac{P(D \mid \theta, G) p(\theta \mid G)}{\int P(D \mid \theta, G) p(\theta \mid G) \, \mathrm{d}\theta} \,. \tag{E-2}$$

If N_{ijk} is the count of $X_i = k$ given π_{ij} in the data D, then the probability of the data given the parameters θ is

$$P(D \mid \theta) = \prod_{i=1}^{n} \prod_{j=1}^{q_i} \prod_{k=1}^{r_i} \theta_{ijk}^{N_{ijk}} \,. \tag{E-3}$$

Let $\theta_{ij} = (\theta_{ij1}, \ldots, \theta_{ijr_i})$. Since θ_{ij} is independent of $\theta_{i'j'}$ when $ij \neq i'j'$, the prior probability of the parameters assuming a fixed structure G is

$$p(\theta \mid G) = \prod_{i=1}^{n} \prod_{j=1}^{q_i} p(\theta_{ij} \mid G) \,. \tag{E-4}$$

The density $p(\theta_{ij} \mid G)$ is a distribution over relative frequencies. Under some very weak assumptions, it is possible to prove that $p(\theta_{ij} \mid G)$ is Dirichlet (see [34], Section 6.2.3). Hence,

$$p(\theta_{ij} \mid G) = \begin{cases} \frac{\Gamma(\alpha_{ij0})}{\prod_{k=1}^{r_i} \Gamma(\alpha_{ijk})} \prod_{k=1}^{r_i} \theta_{ijk}^{\alpha_{ijk}-1} & \text{if } 0 \leq \theta_{ijk} \leq 1 \text{ and } \sum_{k=1}^{r_i} \theta_{ijk} = 1 \\ 0 & \text{otherwise} \end{cases} ,$$

where $\alpha_{ij1}, \ldots, \alpha_{ijr_i}$ are the parameters of the Dirichlet distribution and $\alpha_{ij0} = \sum_{k=1}^{r_i} \alpha_{ijk}$. For the prior to be objective (or noninformative), the parameters α_{ijk} must be identical for all k. Different objective priors have been used in the literature. Cooper and Herskovits [28] use $\alpha_{ijk} = 1$. Heckerman, Geiger, and Chickering [36] use and justify $\alpha_{ijk} = 1/(r_i q_i)$.

It is possible to show that $p(\theta_{ij} \mid D, G)$ is Dirichlet with parameters $\alpha_{ijk} + N_{ijk}, \ldots, \alpha_{ijk} + N_{ijk}$. Hence,

$$p(\theta_{ij} \mid D, G) = \begin{cases} \frac{\Gamma(\alpha_{ij0} + N_{ij})}{\prod_{k=1}^{r_i} \Gamma(\alpha_{ijk} + N_{ijk})} \prod_{k=1}^{r_i} \theta_{ijk}^{\alpha_{ijk}+N_{ijk}-1} & \text{if } 0 \leq \theta_{ijk} \leq 1 \text{ and } \sum_{k=1}^{r_i} \theta_{ijk} = 1 \\ 0 & \text{otherwise} \end{cases} ,$$

where $N_{ij} = \sum_{k=1}^{r_i} N_{ijk}$.

Sampling from a Bayesian network with G known, θ unknown, and D observed involves assigning k to X_i with probability

$$P(X_i = k \mid \pi_{ij}, D, G) = \int \theta_{ijk} p(\theta_{ijk} \mid D, G) \, \mathrm{d}\theta_{ijk} = \frac{\alpha_{ijk} + N_{ijk}}{\sum_{k'=1}^{r_i} (\alpha_{ijk'} + N_{ijk'})} \,. \tag{E-5}$$

E.4 STRUCTURE LEARNING

Finding the most likely structure G that generated a set of data D. The objective is to find the most likely graph given data. By Bayes' rule,

$$P(G \mid D) \propto P(G)P(D \mid G) = P(G) \int P(D \mid \theta, G)p(\theta \mid G) \, \mathrm{d}\theta. \tag{E-6}$$

The previous section explains how to compute the likelihood $P(D \mid \theta, G)$ and the prior $p(\theta \mid G)$. Cooper and Herskovits [28] show how to evaluate the integral above, resulting in

$$P(G \mid D) = P(G) \prod_{i=1}^{n} \prod_{j=1}^{q_i} \frac{\Gamma(\alpha_{ij0})}{\Gamma(\alpha_{ij0} + N_{ij})} \prod_{k=1}^{r_i} \frac{\Gamma(\alpha_{ijk} + N_{ijk})}{\Gamma(\alpha_{ijk})}, \tag{E-7}$$

where $N_{ij} = \sum_{k=1}^{r} N_{ijk}$. Heckerman, Geiger, and Chickering [36] suggest priors over graphs, but it is not uncommon in the literature to assume a uniform prior. For numerical convenience, most Bayesian network learning packages calculate and report $\log P(G \mid D) + K$, where K is a constant independent of G. This quantity is often called the *Bayesian score* and may be used for structure comparison and search.

This page intentionally left blank.

REFERENCES

[1] MITRE, "System safety study of minimum TCAS II," MITRE, Technical Rep. MTR-83W241 (1983).

[2] A. Drumm, "Lincoln Laboratory evaluation of TCAS II Logic Version 6.04a," MIT Lincoln Laboratory, Project Report ATC-240 (1996).

[3] M.P. McLaughlin, "Safety study of the Traffic Alert and Collision Avoidance System (TCAS II)," MITRE Corporation, Technical Rep. MTR 97W32 (1997).

[4] B. Chludzinski, "Lincoln Laboratory evaluation of TCAS II logic version 7," MIT Lincoln Laboratory, Project Report ATC-268 (1999).

[5] "Surveillance and collision avoidance systems," in *Annex 10 to the Convention on International Civil Aviation: Aeronautical Telecommunications*, ICAO, vol. IV, 4th ed. (2007).

[6] M. Edwards, M. Kochenderfer, J. Kuchar, and L. Espindle, "Encounter models for unconventional aircraft," MIT Lincoln Laboratory, Lexington, Massachusetts, Project Report ATC-348 (2009).

[7] M. Kochenderfer, J. Kuchar, L. Espindle, and J. Griffith, "Uncorrelated encounter model of the National Airspace System version 1.0," MIT Lincoln Laboratory, Lexington, Massachusetts, Project Report ATC-345 (2008).

[8] M. Kochenderfer, L. Espindle, J. Kuchar, and J. Griffith, "Correlated encounter model for cooperative aircraft in the National Airspace System version 1.0," MIT Lincoln Laboratory, Lexington, Massachusetts, Project Report ATC-344 (2008).

[9] Federal Aviation Administration, "General Aviation and Part 135 Activity Surveys," http://www.faa.gov/data_statistics/aviation_data_statistics/general_aviation/CY2006/ (2006).

[10] "Sense and Avoid for Unmanned Aircraft Systems," Federal Aviation Administration sponsored Sense and Avoid Workshop, Final report (2009).

[11] J.R. Stanton, "Unmanned Aircraft Systems in homeland security applications," in *48th AIAA Aerospace Sciences Meeting and Exposition*, Orlando, Florida: American Institute of Aeronautics and Astronautics (2010).

[12] "Department of Defense dictionary of military and associated terms," U.S. Department of Defense, Washington, DC, Joint Publication JP 1-02 (2009).

[13] M.J. Kochenderfer, L.P. Espindle, J.K. Kuchar, and J.D. Griffith, "A comprehensive aircraft encounter model of the National Airspace System," *Lincoln Laboratory Journal* 17(2), 41–53 (2008).

[14] M.J. Kochenderfer, L.P. Espindle, M.W.M. Edwards, J.K. Kuchar, and J.D. Griffith, "Airspace encounter models for conventional and unconventional aircraft," in *USA/Europe Air Traffic Management Research and Development Seminar*, Napa, California (2009), vol. 8.

[15] M.J. Kochenderfer, M.W.M. Edwards, L.P. Espindle, J.K. Kuchar, and J.D. Griffith, "Airspace encounter models for estimating collision risk," *Journal of Guidance, Control, and Dynamics* 33(2), 487–499 (2010).

[16] "World Vector Shoreline (WVSPLUS)," National Imagery and Mapping Agency, Bethesda, MD, Performance Specification MIL-PRF-0089012A (1999).

[17] M.P. McLaughlin and A.D. Zeitlin, "Safety study of TCAS II for logic version 6.04," MITRE Corporation, Technical Rep. MTR92W102 (1992).

[18] T.A. Choyce and K.M. Ciaramella, "Test and evaluation of TCAS II logic version 7," Federal Aviation Administration, Technical rep. (2000).

[19] T. Miquel and K. Rigotti, "European encounter model," CENA/Sofréavia and QinetiQ, Technical Rep. ACASA/WP1/186/D (2002).

[20] S. Chabert, "Safety encounter model focused on issue SA01a," CENA/Sofréavia and QinetiQ, Technical Rep. SIRE/WP2/21/D (2005).

[21] H. Hutchinson, "Implications on ACAS performances due to ASAS implementation," Eurocontrol, Technical Rep. IAPA/WP10 (2005).

[22] B. Raynaud and T. Arino, "Final report on the safety of ACAS II in the European RVSM environment," Eurocontrol, Technical Rep. ASARP/WP9/72/D (2006).

[23] R. Srinivasan, *Importance Sampling: Applications in Communications and Detection*, Springer (2002).

[24] M.J. Evans and J.S. Rosenthal, *Probability and Statistics: The Science of Uncertainty*, New York: W. H. Freeman, 1st ed. (2004).

[25] D.H. Johnson, "The insignificance of statistical significance testing," *The Journal of Wildlife Management* 63(3), 763–772 (1999), URL http://www.jstor.org/stable/3802789.

[26] D.J. Spiegelhalter, N.G. Best, B.P. Carlin, and A.v.d. Linde, "Bayesian measures of model complexity and fit," *Journal of the Royal Statistical Society. Series B (Statistical Methodology)* 64(4), 583–639 (2002), URL http://www.jstor.org/stable/3088806.

[27] M. Hamada, A. Wilson, C. Reese, and H. Martz, *Bayesian Reliability*, Springer (2008).

[28] G.F. Cooper and E. Herskovits, "A Bayesian method for the induction of probabilistic networks from data," *Machine Learning* 9(4), 309–347 (1992).

[29] L. Espindle and M. Kochenderfer, "Classification of primary radar tracks using Gaussian mixture models," *IET Radar, Sonar and Navigation* 3(6), 559–568 (2009).

[30] J.P. Chryssanthacopoulos, J.K. Kuchar, J.J. Scillieri, and R.E. Williams, "Radar multiangulation for altitude inference," MIT Lincoln Laboratory, Lexington, Massachusetts, Project Report ATC-357 (2009).

[31] G. May, "A method for predicting the number of near mid-air collisions in a defined airspace," *Journal of the Operational Research Society* 22, 237–251 (1971).

[32] J. Pearl, *Probabilistic Reasoning in Intelligent Systems: Networks of Plausible Inference*, San Francisco, CA: Morgan Kaufmann (1988).

[33] F.V. Jensen, *Bayesian Networks and Decision Graphs*, Springer Verlag (2001).

[34] R.E. Neapolitan, *Learning Bayesian Networks*, Upper Saddle River, NJ: Prentice Hall (2004).

[35] T.H. Cormen, C.E. Leiserson, R.L. Rivest, and C. Stein, *Introduction to Algorithms*, MIT Press, 2nd ed. (2001).

[36] D. Heckerman, D. Geiger, and D.M. Chickering, "Learning Bayesian networks: The combination of knowledge and statistical data," *Machine Learning* 20(3), 197–243 (1995).

This page intentionally left blank.

REPORT DOCUMENTATION PAGE

1. REPORT DATE	2. REPORT TYPE	3. DATES COVERED *(From - To)*
15 September 2010	Project Report	

4. TITLE AND SUBTITLE	5a. CONTRACT NUMBER
Encounter Models for the Littoral Regions of the National Airspace System	FA8721-05-C-0002
	5b. GRANT NUMBER
	5c. PROGRAM ELEMENT NUMBER

6. AUTHOR(S)	5d. PROJECT NUMBER
Matthew W. Edwards, Group 42	10082
	5e. TASK NUMBER 1
	5f. WORK UNIT NUMBER

7. PERFORMING ORGANIZATION NAME(S) AND ADDRESS(ES) AND ADDRESS(ES)	8. PERFORMING ORGANIZATION REPORT NUMBER
MIT Lincoln Laboratory 244 Wood Street Lexington, MA 02420-9108	PR-CASSATT-2

9. SPONSORING / MONITORING AGENCY NAME(S) AND ADDRESS(ES)	10. SPONSOR/MONITOR'S ACRONYM(S)
Department of Homeland Security John Appleby	DHS
DHS Science and Technology Washington, DC 20528 Phone 202-254-5842 Fax 202-906-9520	**11. SPONSOR/MONITOR'S REPORT NUMBER(S)** ESC-TR-2010-051

12. DISTRIBUTION / AVAILABILITY STATEMENT

Approved for public release; distribution is unlimited.

13. SUPPLEMENTARY NOTES

14. ABSTRACT

The primary objective of this analysis was the development of a littoral correlated and uncorrelated encounter model for use in collision avoidance and sense and avoid system evaluation. In addition, a methodology was developed to determine whether the models were both distinctive from the continental United States encounter models and sufficient in terms of the quantity of data used to build the models. Application of this methodology demonstrated that both the littoral correlated and uncorrelated model characteristics were different than the previous models and that sufficient data were used to build the models. Lastly, this analysis determined that although the encounter initial conditions tend to vary in a littoral environment, the aircraft dynamic behavior, or how the various aircraft states transition during the encounter, remains the same.

15. SUBJECT TERMS

16. SECURITY CLASSIFICATION OF:			17. LIMITATION OF ABSTRACT	18. NUMBER OF PAGES	19a. NAME OF RESPONSIBLE PERSON
a. REPORT Unclassified	**b. ABSTRACT** Unclassified	**c. THIS PAGE** Unclassified	Same as report	83	**19b. TELEPHONE NUMBER** *(include area code)*

This page intentionally left blank.